Inelastic scattering - II

Core loss spectroscopy

Cécile Hébert IPHYS-LSME

Layout

- Introduction
- Double differential scattering cross section
- Quantification
- ELNES
- Angular resolved EELS
- Dichroisim in the TEM

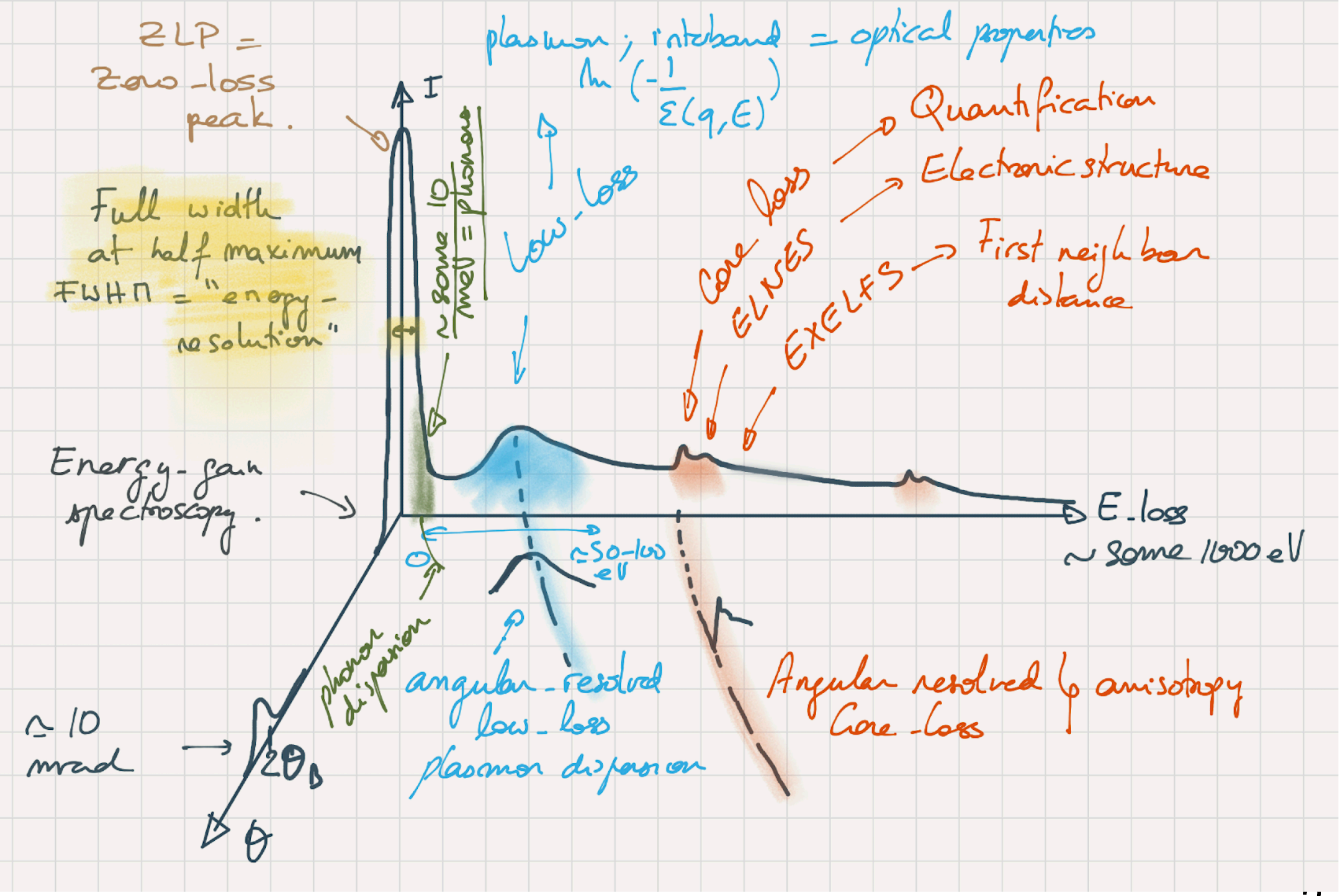

Dipole approximation

$$\frac{\partial^2\sigma}{\partial E\,\partial\Omega} \propto \frac{k'}{k_0}\frac{1}{q^4}\sum_F |\langle I|\underbrace{\overbrace{e^{2\pi i\vec{q}\cdot\vec{R}}}^{\ll 1}}_{\simeq\, 1 + i2\pi\vec{q}\cdot\vec{R}}|F\rangle|^2\,\delta(E_F - E_I - \Delta E)$$

$$\to \underbrace{\cancel{\langle I|F\rangle}}_{0} + |\langle I|\vec{q}\cdot\vec{R}|F\rangle|^2$$

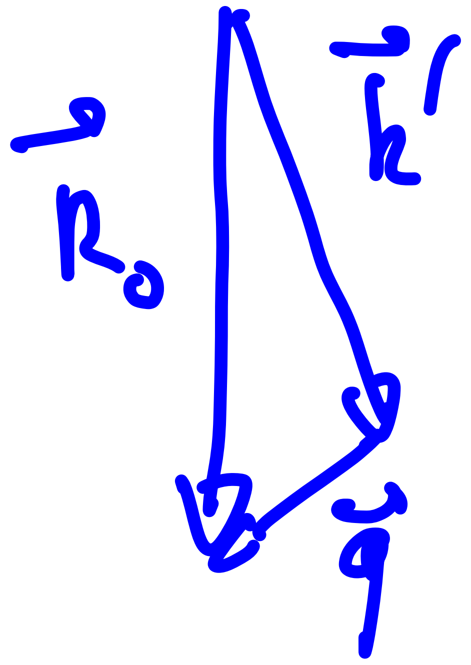

$$\frac{\partial^2\sigma}{\partial E\,\partial\Omega} \propto \frac{1}{q^4}\sum_F |\langle I|\vec{q}\cdot\vec{R}\,|F\rangle|^2\,\delta(E_F - E_I - \Delta E)$$

$\Delta l = \pm 1$

Dipole selection rule. Usually OK.

$s \to p$ K edge (L_1 edge)

$p \to s$, $p \to d$ ... L_{23} edge ...

Dipole approximation: link with XANES

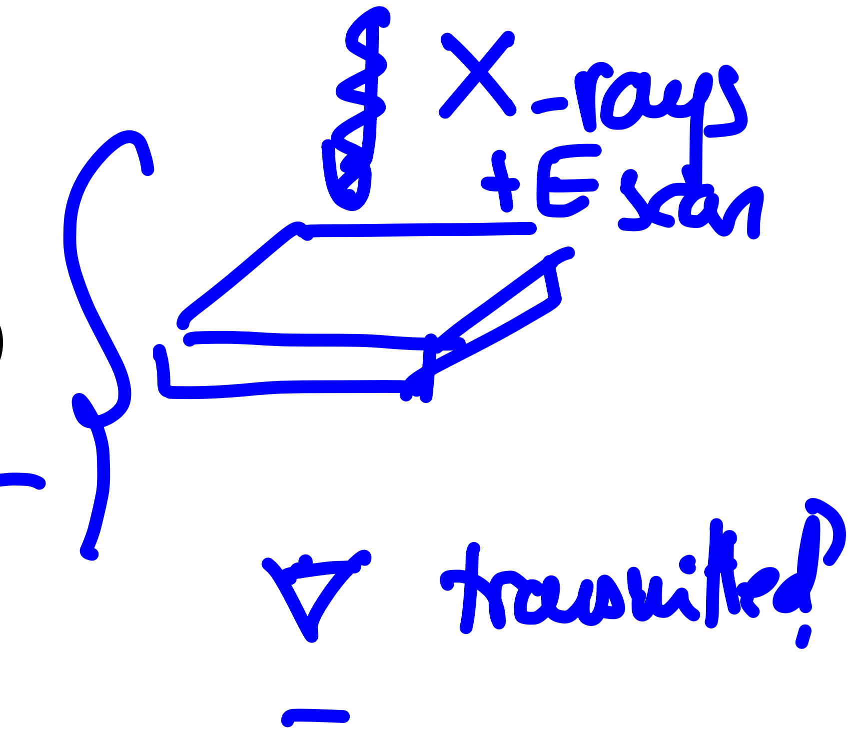

Absorbtion

$$\frac{\partial^2\sigma}{\partial E\,\partial\Omega} \propto \frac{1}{q^4}\sum_F |\langle I|\vec{q}\cdot\vec{R}\,|F\rangle|^2\,\delta(E_F - E_I - \Delta E)$$

Equivalent to the dipole transition in XANES, with $\vec{q} <-> \vec{e}$ polarisation vector

Angular dependence of X-ray absorption spectra
C Brouder , Journal of Physics: Condensed Matter, Volume 2, Number 3, 1990

A1.1. Dipole transitions

The dipole absorption cross section can be written

polarisation vector of the light

$$\sigma^{\mathrm{D}}(\hat{\varepsilon}) = 4\pi^2\alpha\hbar\omega \sum_{\mathrm{if}} |\langle \mathrm{f}|\hat{\varepsilon}\cdot \boldsymbol{r}|\mathrm{i}\rangle|^2\,\delta(E_{\mathrm{f}} - E_{\mathrm{i}} - \hbar\omega) = \sum_{ij} \varepsilon_i\varepsilon_j\sigma^{ij}. \qquad \text{(A1)}$$

Magnetic circular dichroism

Instead of linearly polarized light → circularly polarized light

- ➢Prediciton: Erskine and Stern, PRB 12, (1975) 737
- ➢Experimental verification (Fe K edge): Schütz et al., PRL 58, (1987) 737
- ➢Breakthrough (Fe L edge): Chen et al. PRL 75, (1995) 152-155.

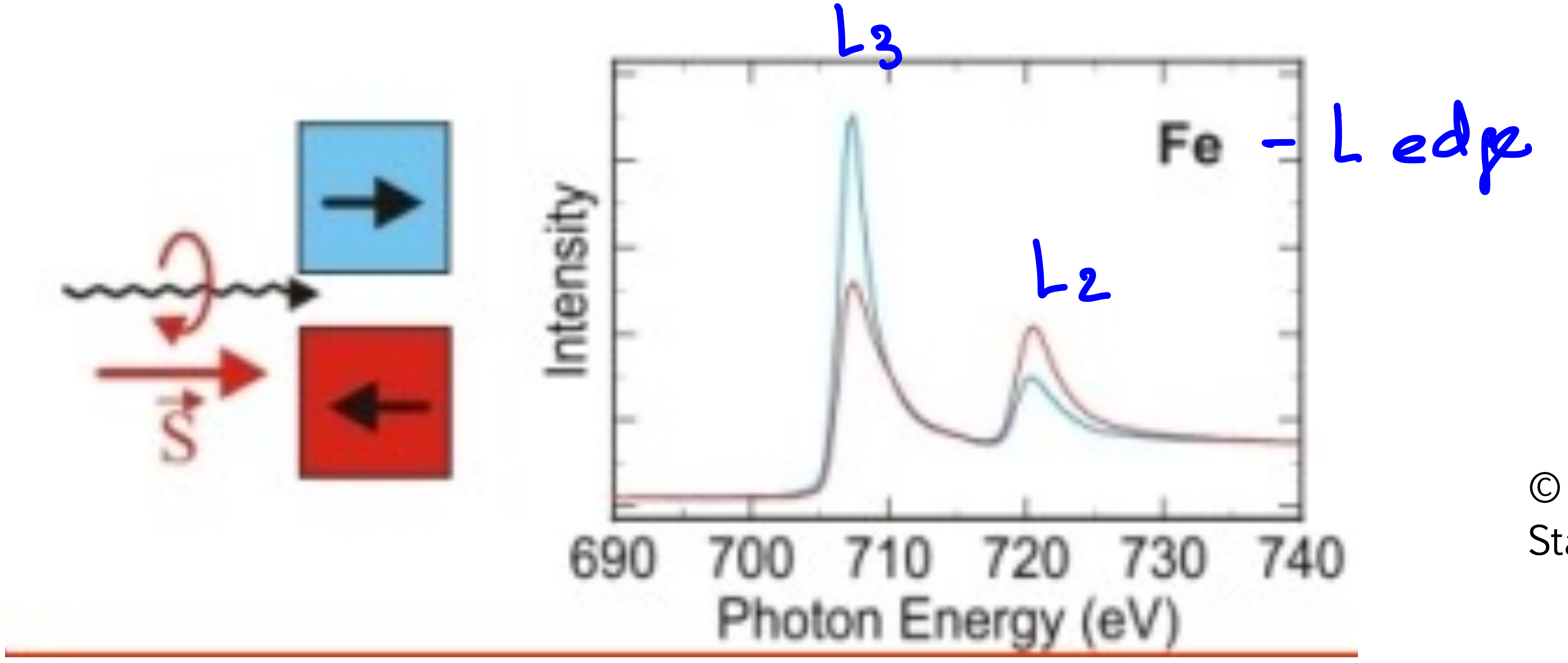

© J. Stöhr, Stanford

Magnetic circular dichroism

Circular dichroism in $L_{2,3}$ edges of d-metals schematic

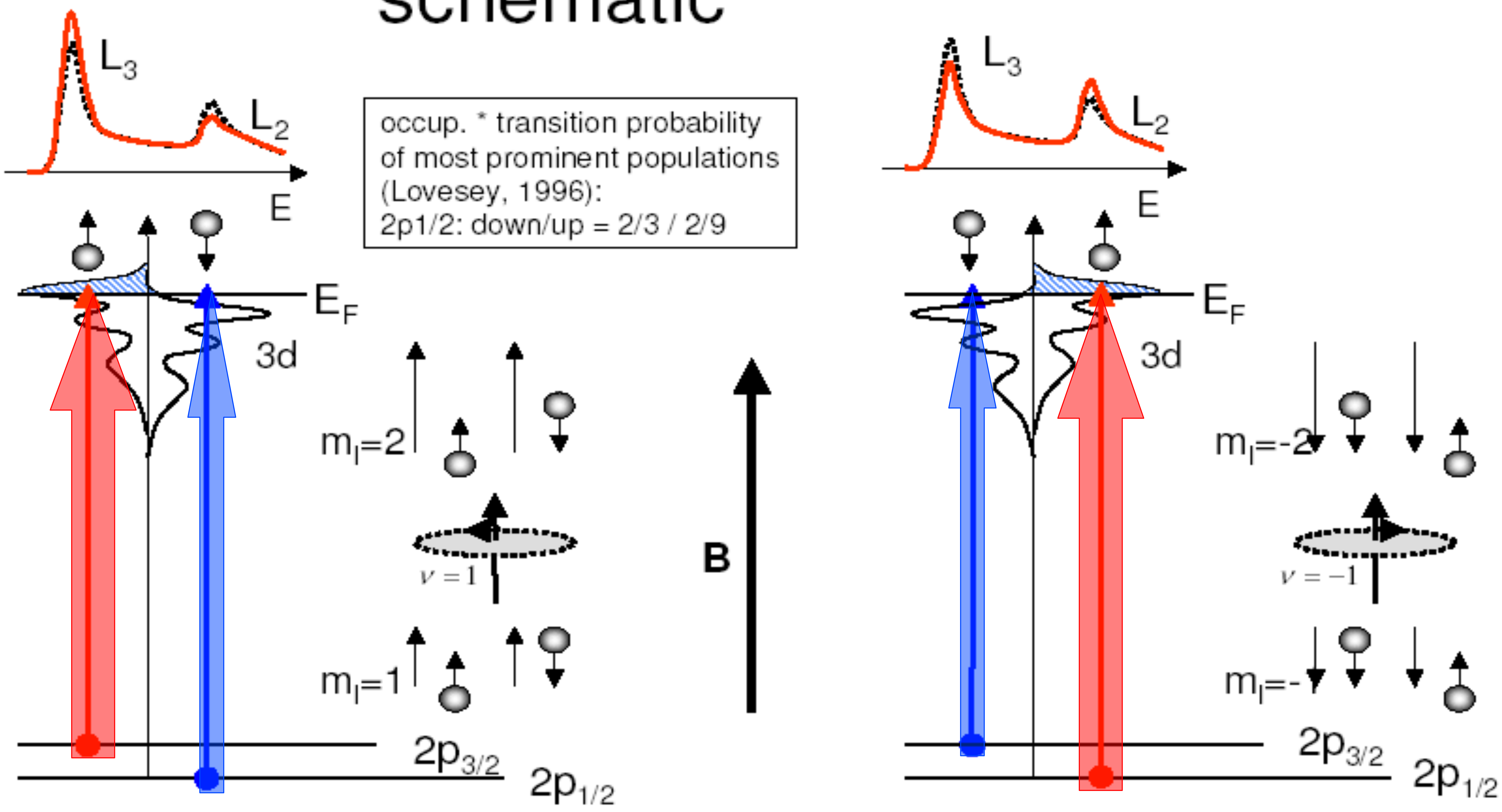

occup. * transition probability
of most prominent populations
(Lovesey, 1996):
2p1/2: down/up = 2/3 / 2/9

Magnetic circular dichroism

$\vec{\varepsilon}_1$ $\vec{\varepsilon}_2$ phase shift $\frac{\pi}{2}$

Polarization vector in XANES $\triangleq$ Momentum transfer q in ELNES

$$\vec{\varepsilon}_1 + i\vec{\varepsilon}_2 \qquad\qquad \vec{q} + i\vec{q}'$$

with $\vec{q} \perp \vec{q}'$

Matrix elements of DFF in dipole approximation:

$$\sum_{i,f} \left|\langle f|(\vec{q}+i\vec{q}')\cdot\hat{R}|i\rangle\right|^2 =$$

$$\sum_{i,f} \left|\langle f|\vec{q}\cdot\hat{R}|i\rangle\right|^2 + \sum_{i,f} \left|\langle f|\vec{q}'\cdot\hat{R}|i\rangle\right|^2 + i\left\{\sum_{i,f}\langle i|\vec{q}'\cdot\hat{R}|f\rangle\langle f|\vec{q}\cdot\hat{R}|i\rangle - \sum_{i,f}\langle i|\vec{q}\cdot\hat{R}|f\rangle\langle f|\vec{q}'\cdot\hat{R}|i\rangle\right\}$$

$$\propto \Im\left\{\mathrm{MDFF}(\vec{q},\vec{q}',E)\right\} \propto \vec{q}\wedge\vec{q}'$$

↳ max. of

Non zero only for magnetic transitions

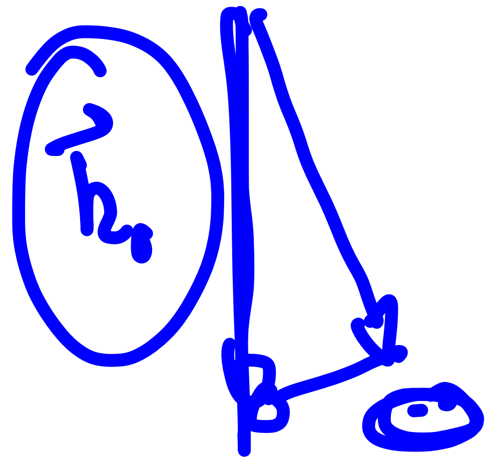

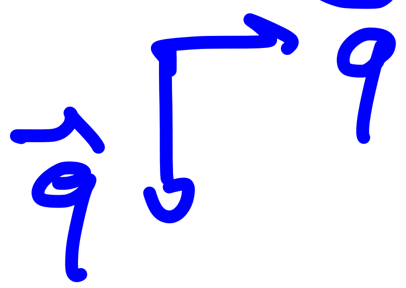

Magnetic circular dichroism

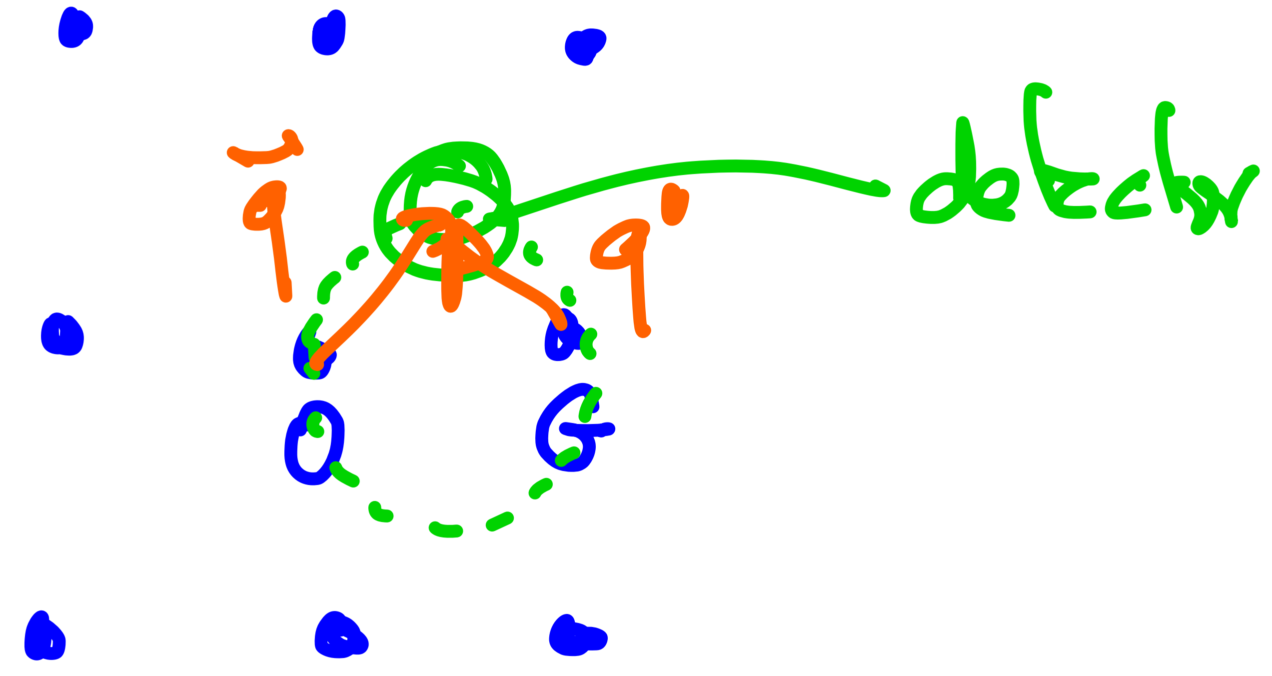

$$\cancel{\sum_{i,f}\left|\langle f|\vec{q}\cdot\hat{R}|i\rangle\right|^2+\sum_{i,f}\left|\langle f|\vec{q}'\cdot\hat{R}|i\rangle\right|^2}+2\text{x}\; i\left\{\sum_{i,f}\langle i|\vec{q}'\cdot\hat{R}|f\rangle\langle f|\vec{q}\cdot\hat{R}|i\rangle-\sum_{i,f}\langle i|\vec{q}\cdot\hat{R}|f\rangle\langle f|\vec{q}'\cdot\hat{R}|i\rangle\right\}$$

$$\propto \vec{q}\wedge\vec{q}'$$

Change phase shift from
+π/2 to −π/2

$$\vec{q}+i\vec{q}' \;\longrightarrow\; \vec{q}-i\vec{q}'$$

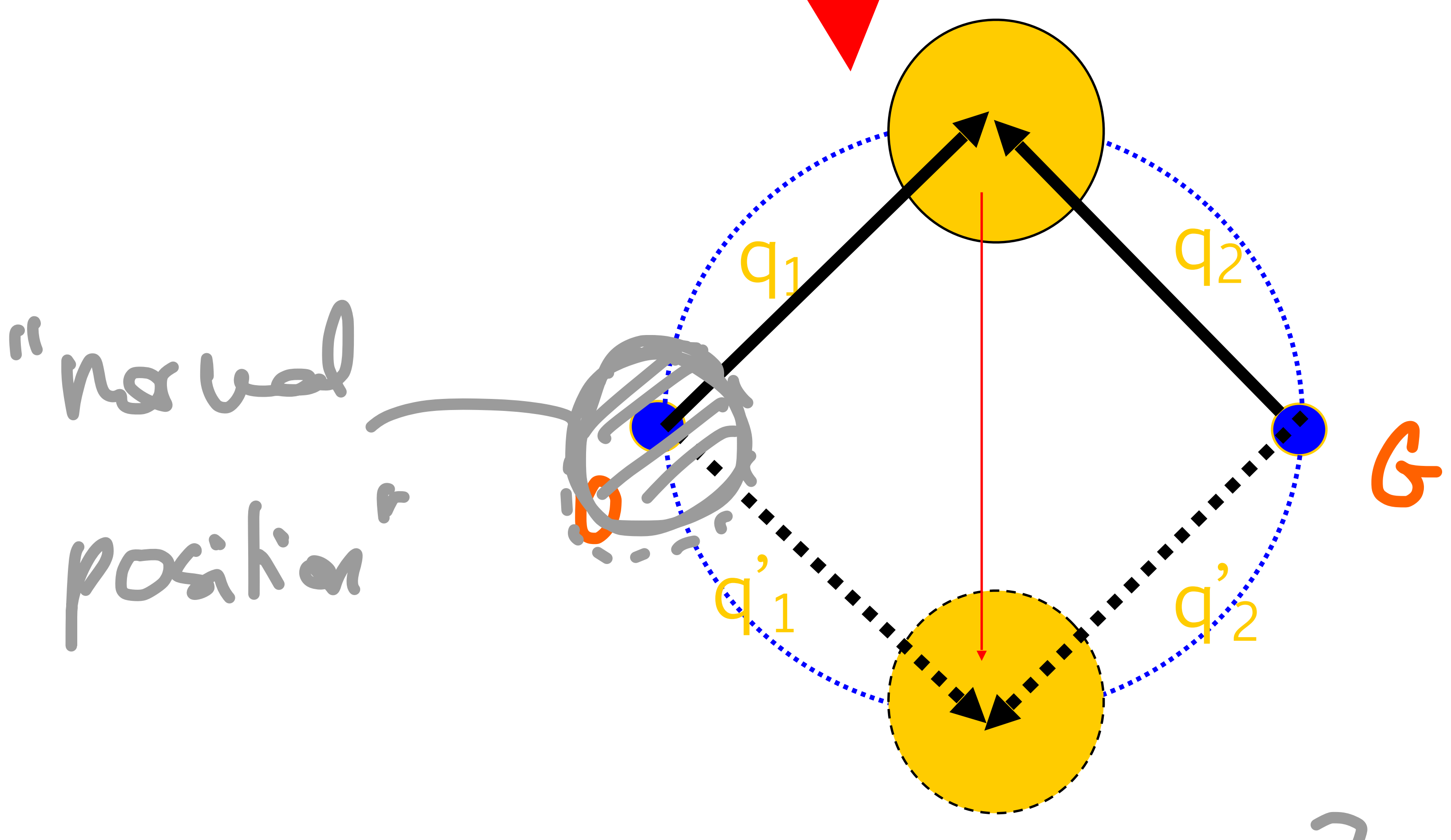

$\vec{q} \perp \vec{q}'$ ¿

phase shift
≈ ok

V with thickness

Magnetic circular dichroism

Laue circle centre and thickness determine phase shift

$$\frac{\partial^2\sigma}{\partial E\,\partial\Omega} = \frac{4\gamma^2}{a_0^2}\frac{k_f}{k_i}\left\{\sum_{j=1}^{2n}\frac{\mathrm{DFF}(\vec{q}_j,E)}{q_j^4} + \sum_{i\neq j} C_{ij}\frac{\mathrm{MDFF}(\vec{q}_i,\vec{q}_j,E)}{q_i^2 q_j^2}\right\}$$

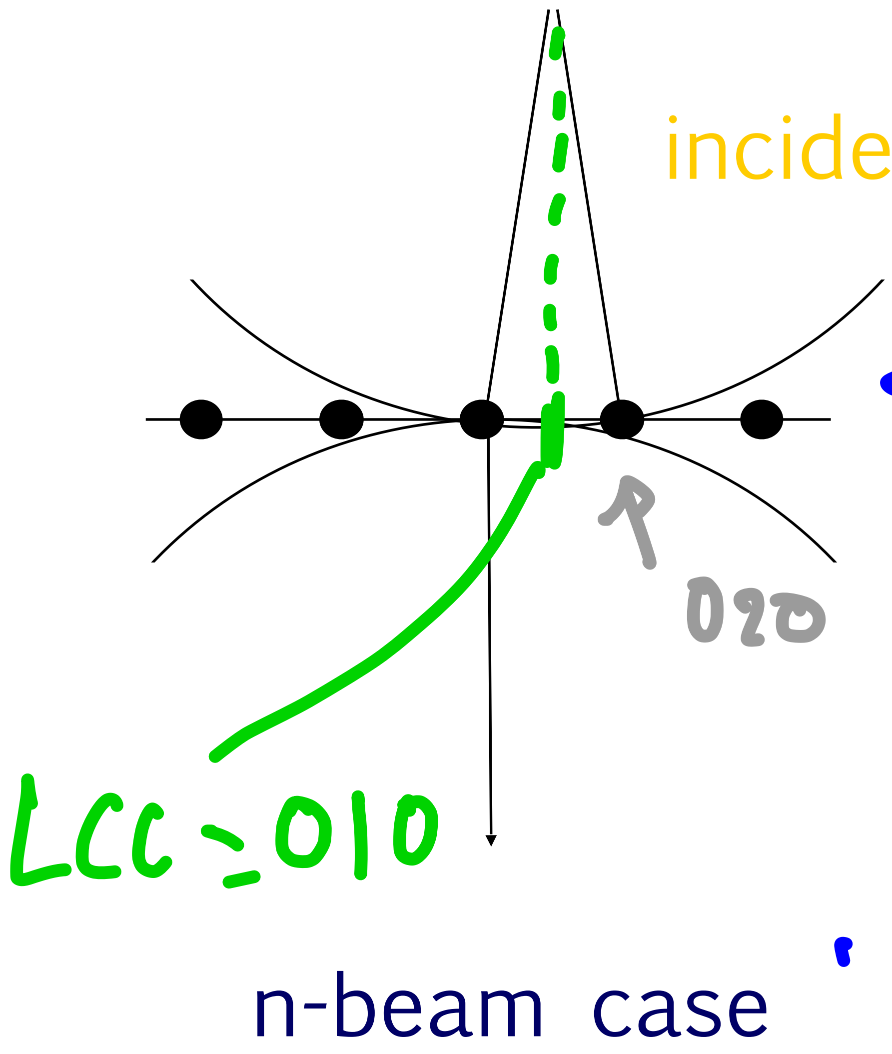

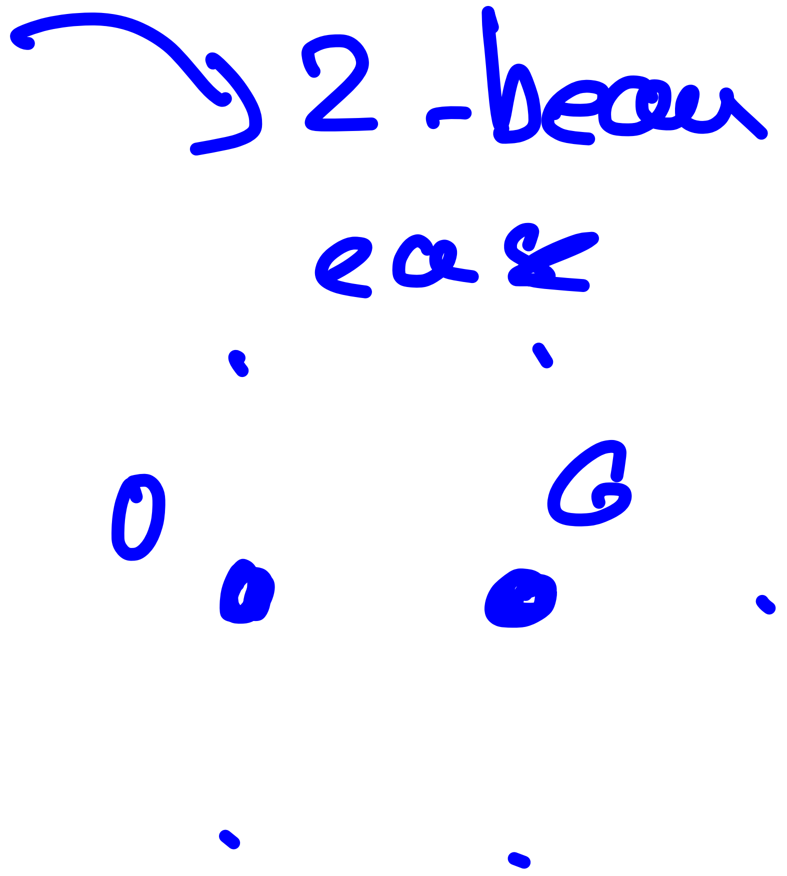

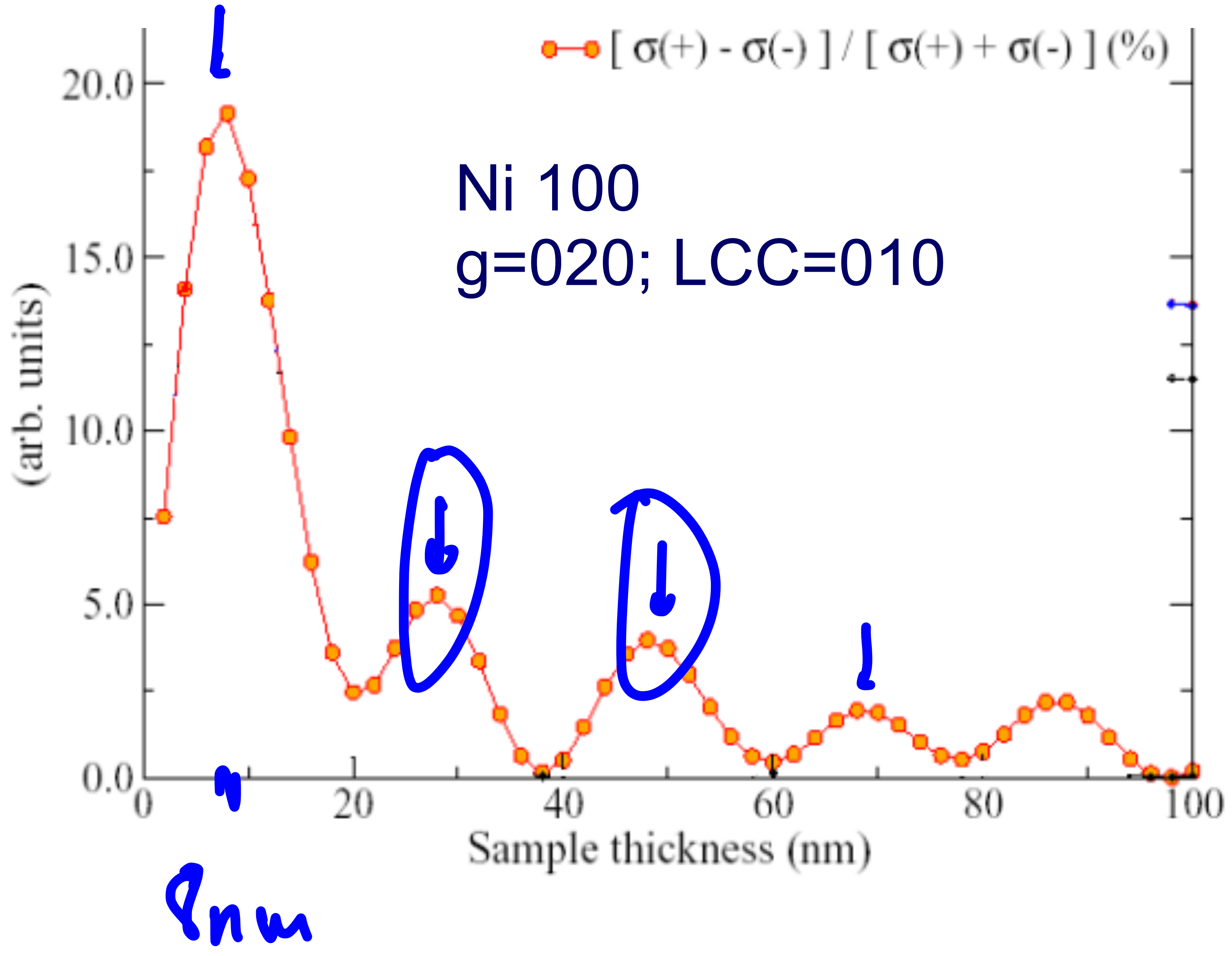

Magnetic circular dichroism

Ni

loss intensity

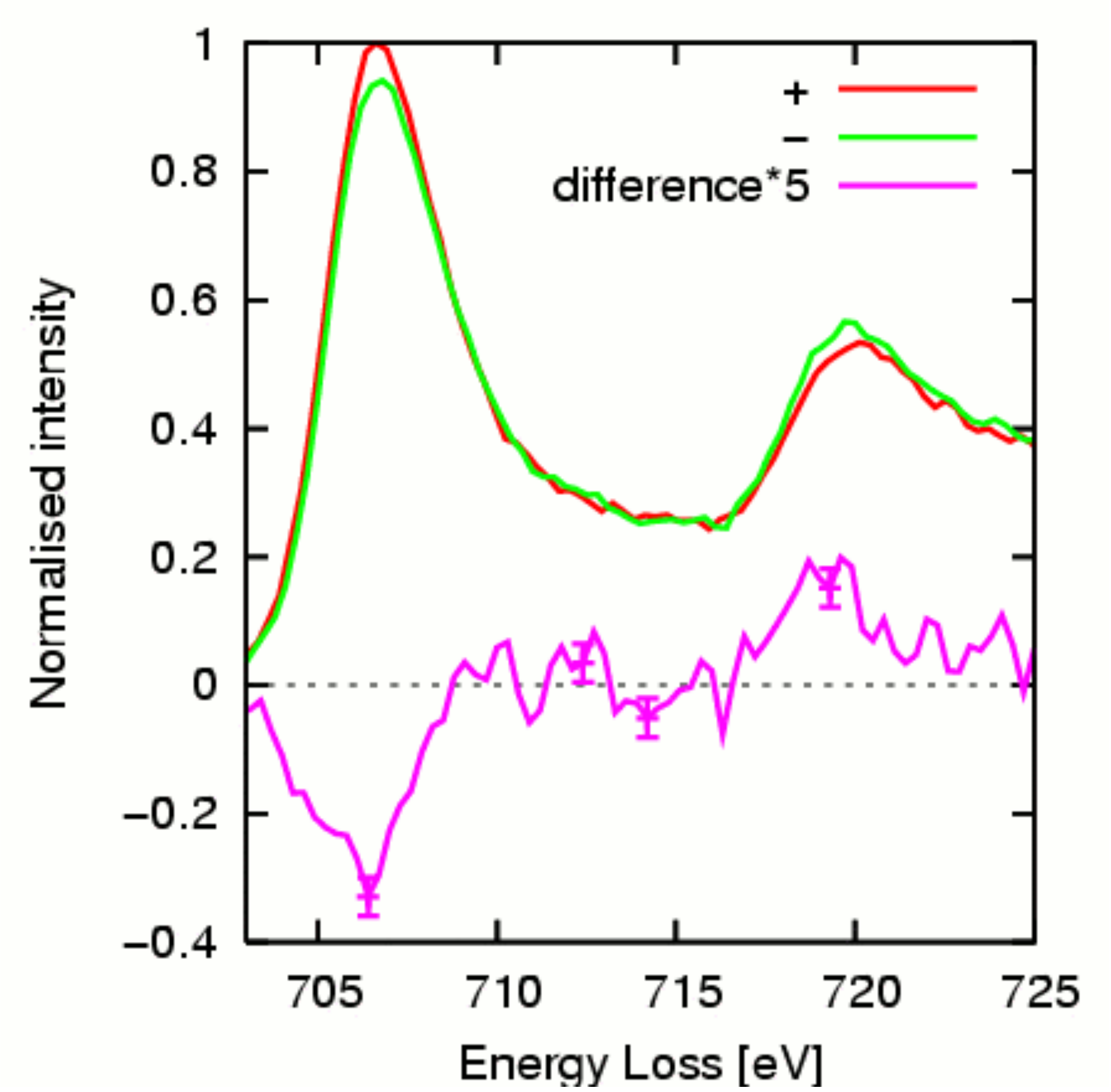

EMCD

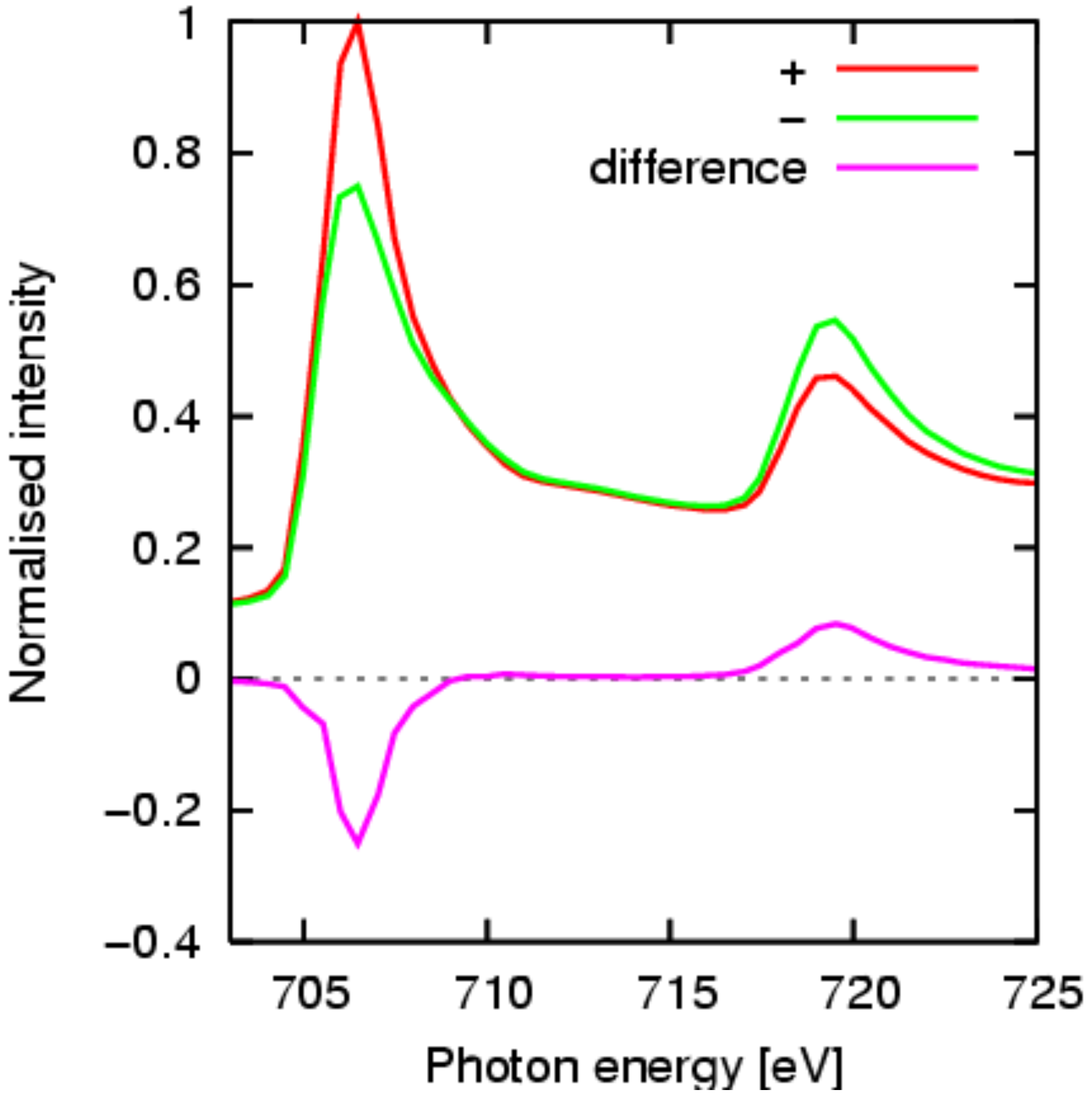

XMCD

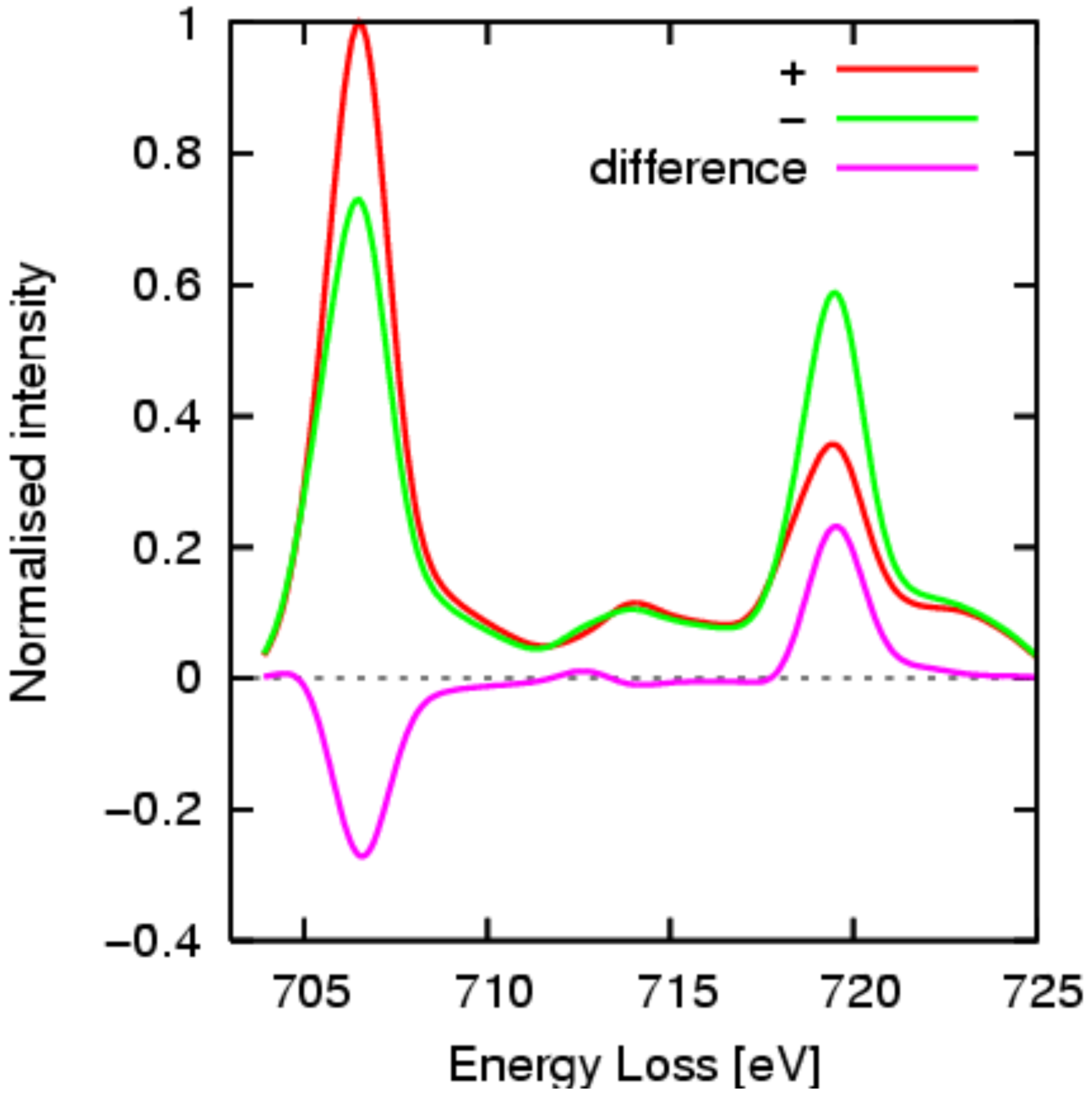

WIEN2k calc.

- ➢EMCD (exposure 60 s, 200 nm): S. Rubino, TU Vienna
- ➢Specimen and XMCD: E. Carlino et al., TASC, Elettra
- ➢Calculation: P. Novak et al., Inst. of Physics, Prague

P. Schattschneider et al., Nature 441,486-488

Magnetic circular dichroism

Thickness dependence

Cobalt single crystal

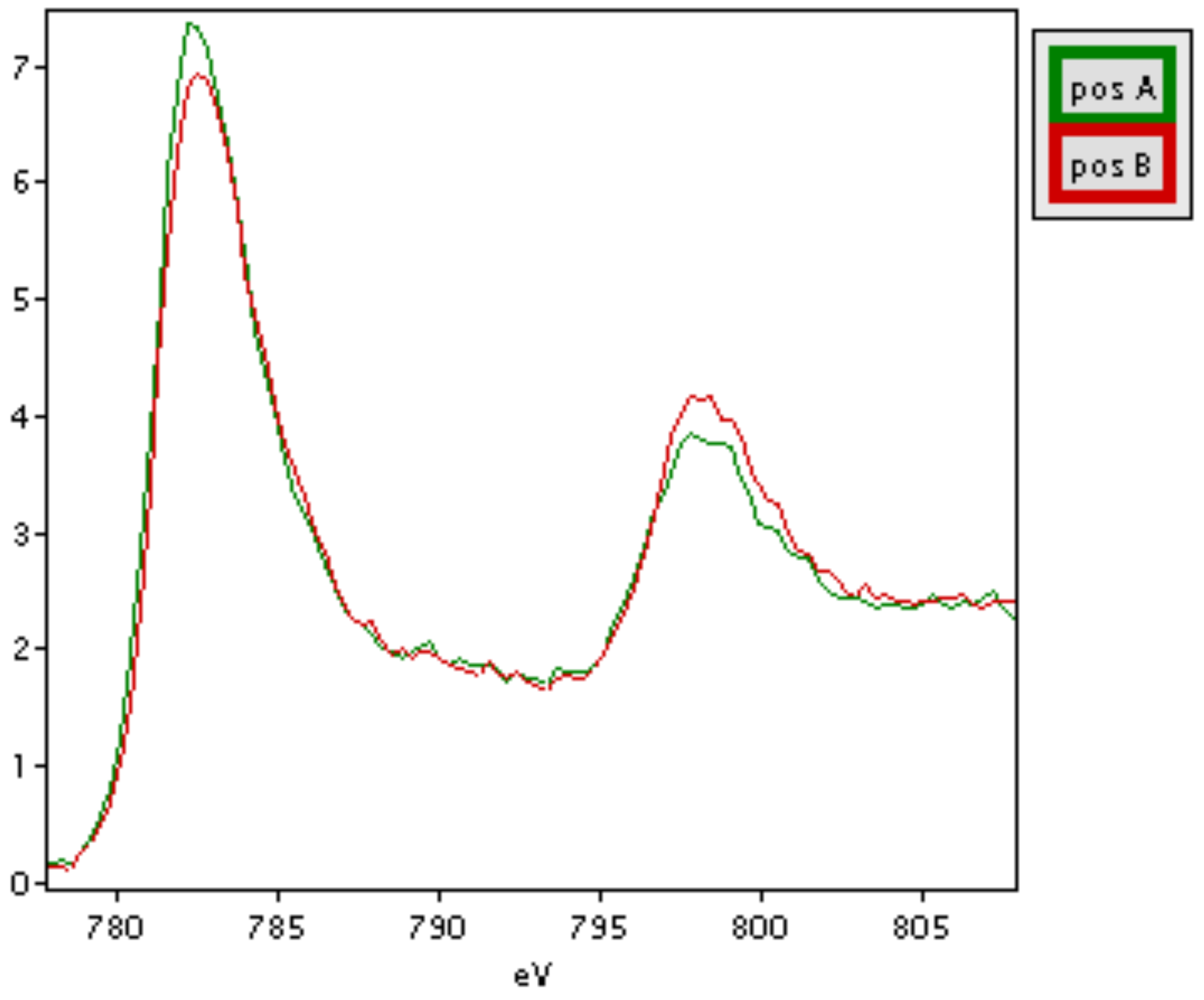

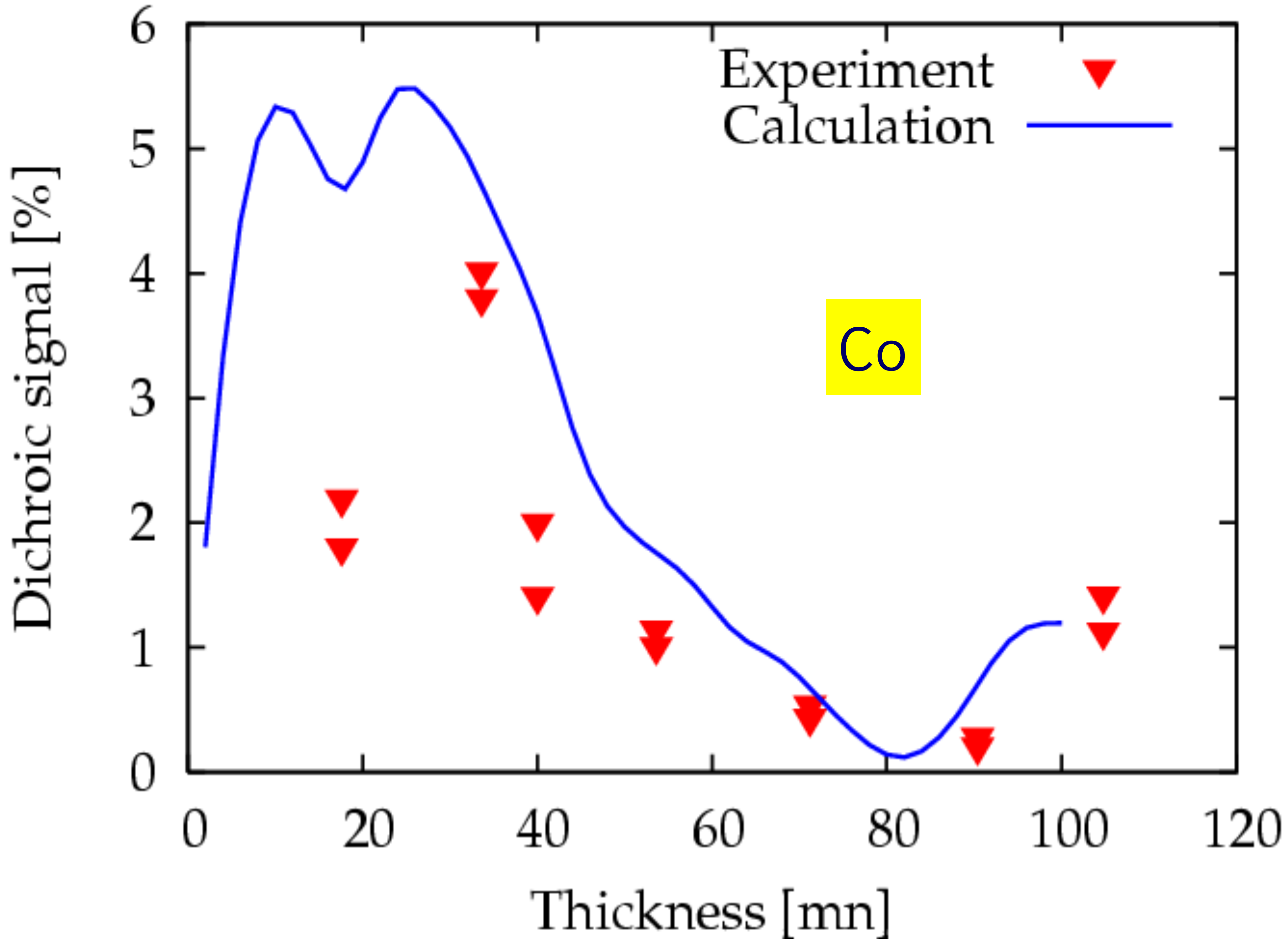

2006: Detector shift method
Co [001] g= 1,0,0 LCC=1/2,0,0
200 nm lateral resolution
Optimized illumination
60 s acquisition time

Magnetic circular dichroism

Convergent beam? V

intensity ↗ → signal ↗ SNR ↗

signal to background ↘

MICROSCOPY

Microscopy, 2018, i60–i71
doi: 10.1093/jmicro/dfx129
Advance Access Publication Date: 23 January 2018

Article

Convergent-beam EMCD: benefits, pitfalls and applications

S. Löffler[1,2,*] and W. Hetaba[1,3]

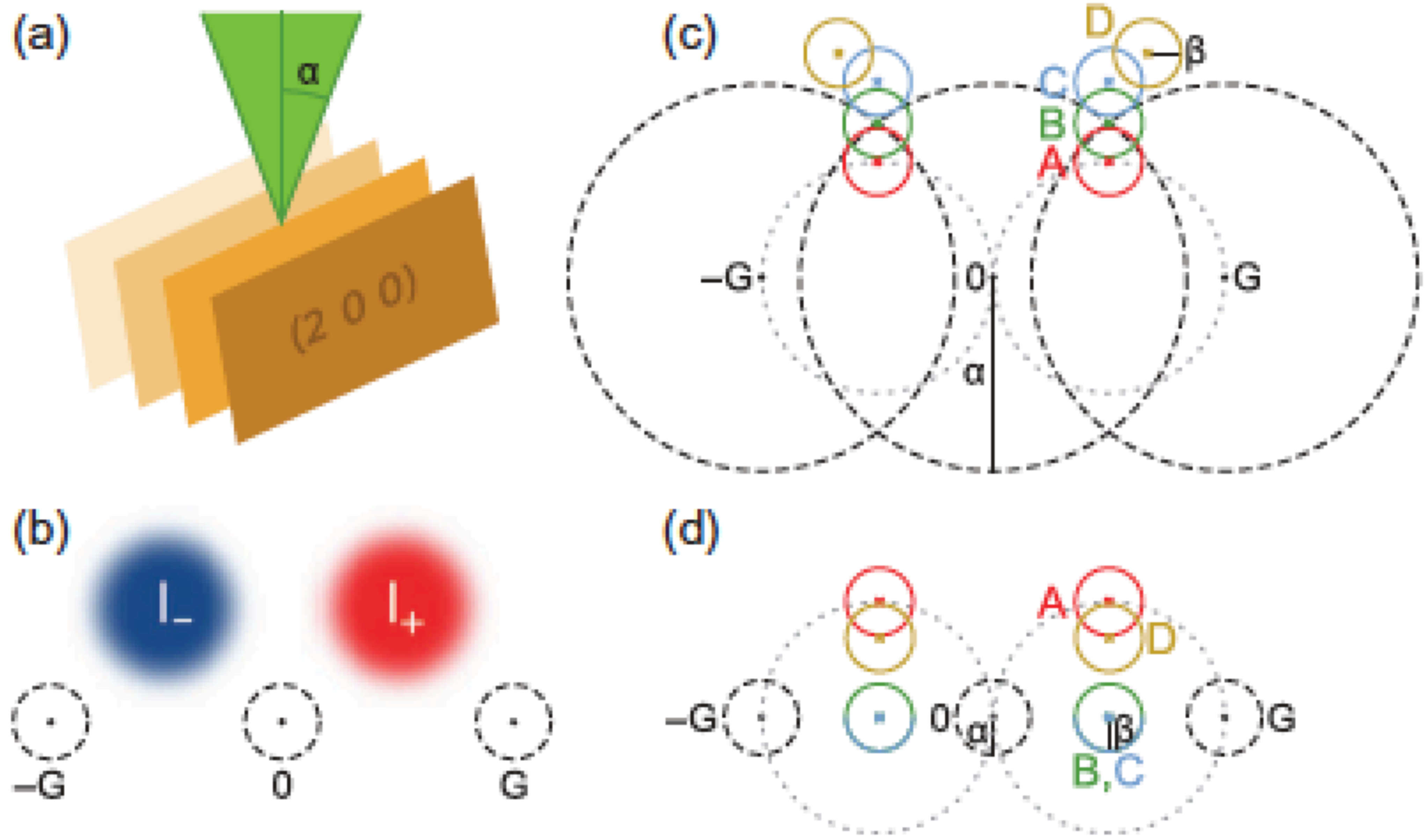

BCC Fe 10 nm
300 kV
10° from [100]
020 spot (systematic row

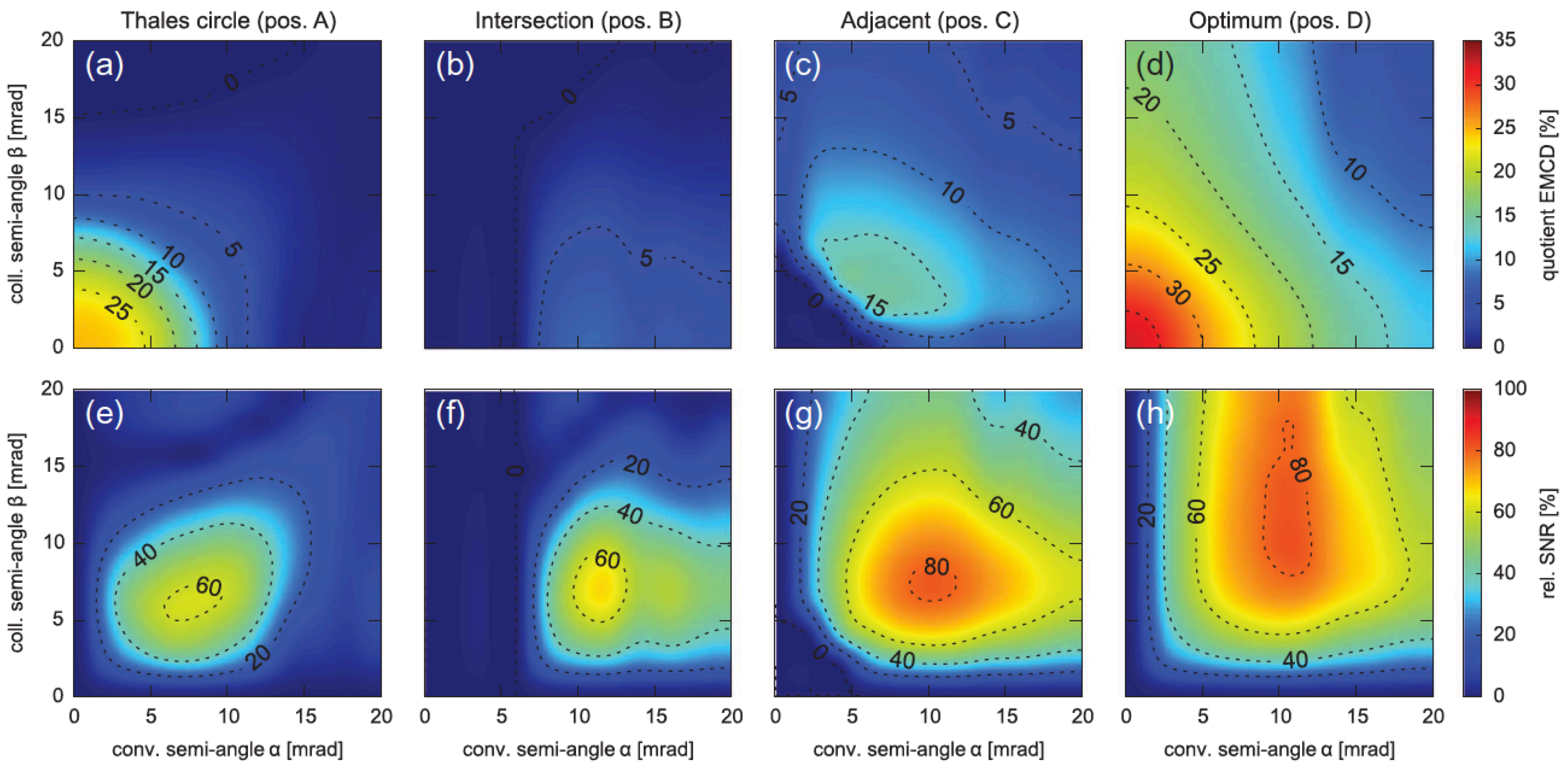

Fig. 4. EMCD effect S (a–d) and SNR $S/\delta S$ (e–h) for the four sets of detector positions A–D as a function of convergence and collection semi-angles. The SNR is given for a jump ratio of r = 2 in fractions of the maximum SNR.

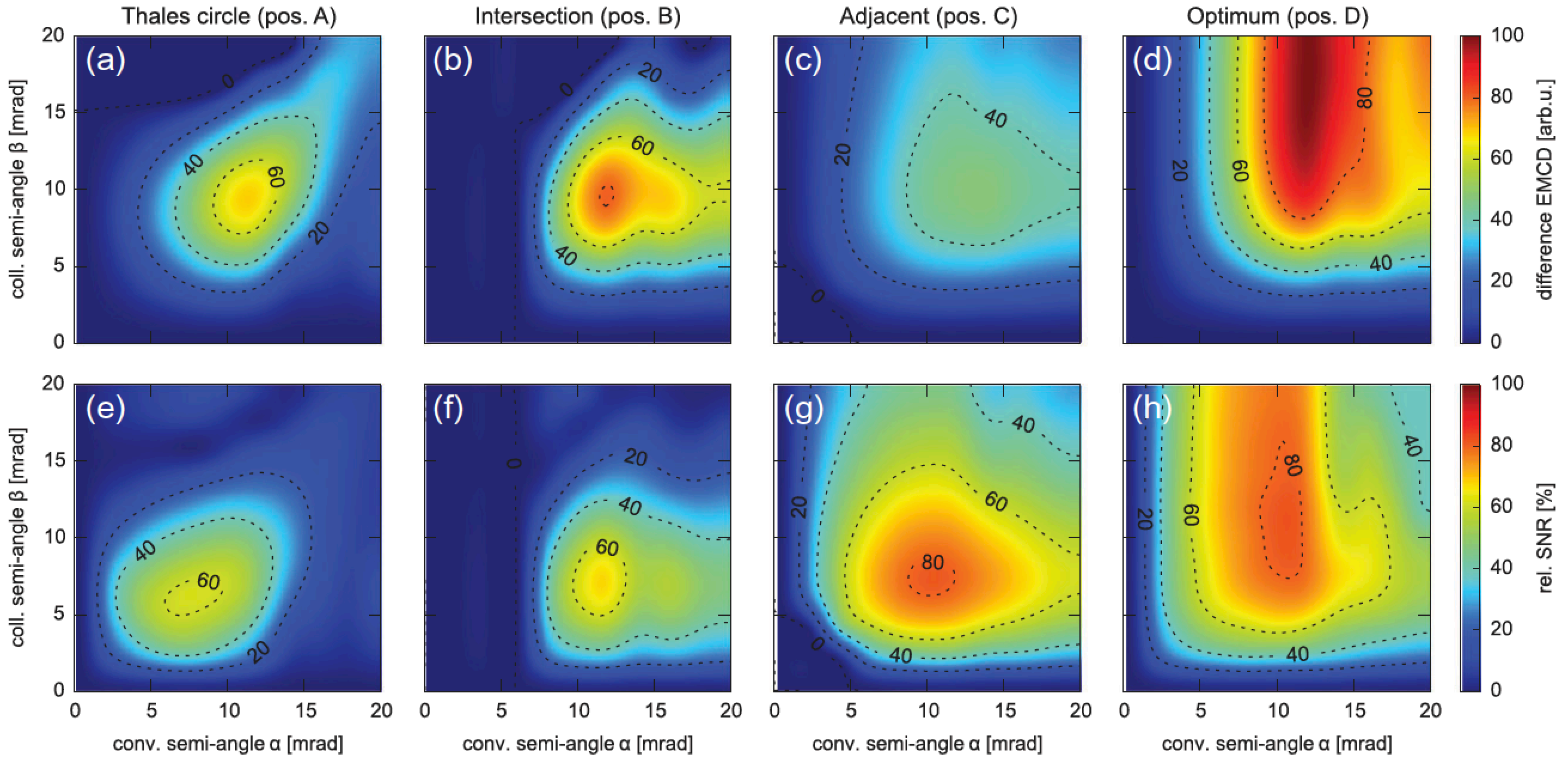

Fig. 3. Difference signal ΔI (a–d) and SNR $\Delta I/\delta\Delta I$ (e–h) for the four sets of detector positions A–D as a function of convergence and collection semi-angles. The SNR is given for a jump ratio of $r = 2$ in fractions of the maximum SNR.

ARTICLE

Received 31 May 2016 | Accepted 21 Jul 2016 | Published 31 Aug 2016

DOI: 10.1038/ncomms12672

OPEN

Magnetic measurements with atomic-plane resolution

Ján Rusz[1], Shunsuke Muto[2], Jakob Spiegelberg[1], Roman Adam[3], Kazuyoshi Tatsumi[2], Daniel E. Bürgler[3], Peter M. Oppeneer[1] & Claus M. Schneider[3]

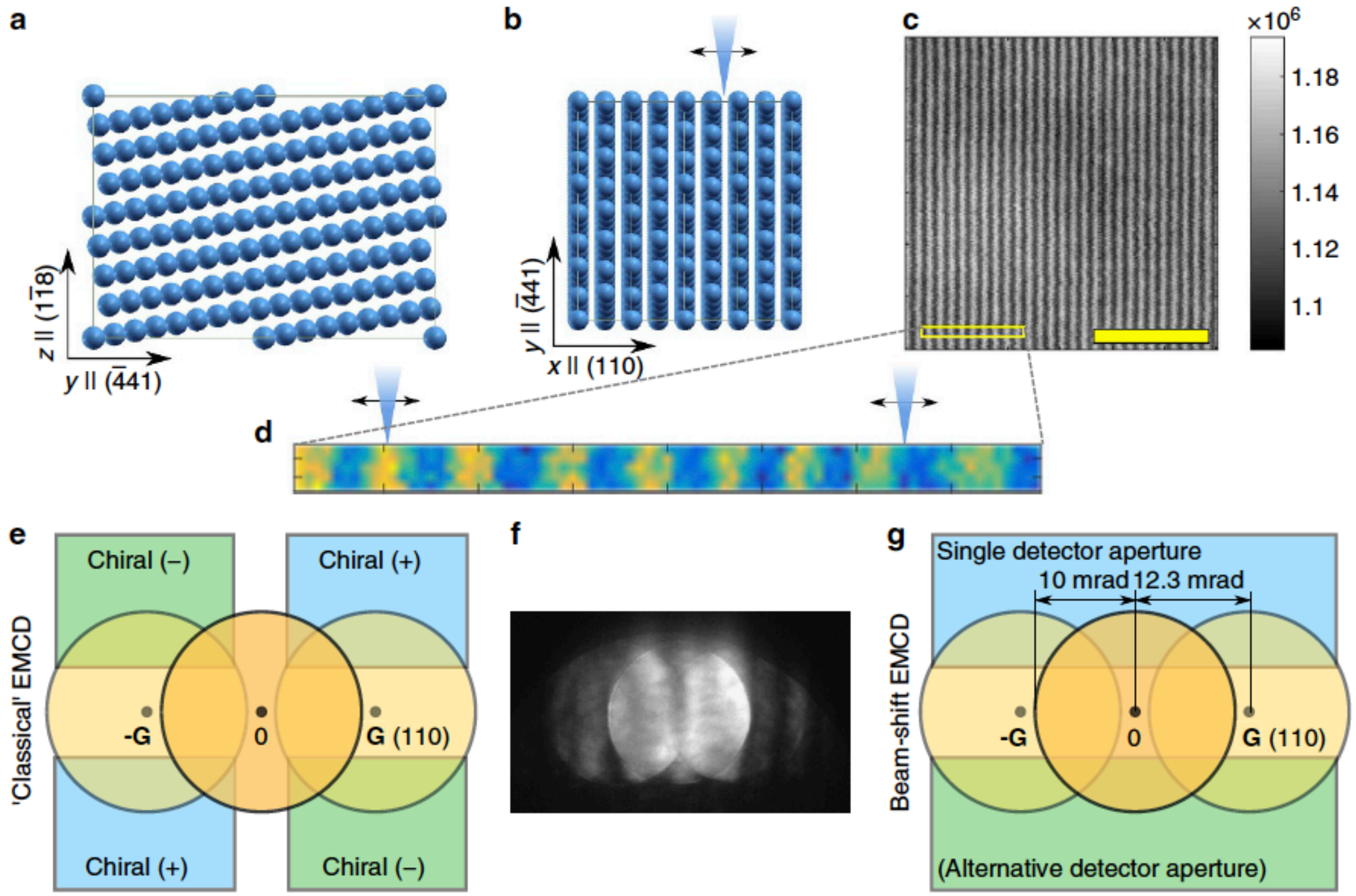

Figure 1 | Scheme of the experimental set-up. (**a**) Side-view of the structure model of bcc iron tilted into a 3-beam orientation with the beam along the (1$\bar{1}$8) direction. (**b**) Top view of the structure model. Scanning direction is schematically shown by blue cone with arrows. (**c**) ADF survey image (acceleration voltage 200 kV, convergence semi-angle 10 mrad) showing atomic planes. The yellow scale bar denotes 2 Å. (**d**) ADF image acquired along with the acquisition of a spectrum image. Its size corresponds to the yellow rectangle marked in the ADF survey image. (**e**) Schematic placement of detectors for a classical EMCD approach in the 3-beam orientation. (**f**) Experimental diffraction pattern acquired in the same settings as the ADF survey image. (**g**) Detector placement in the here-proposed APR-EMCD approach. Note that in the classical approach we need two measurements at each beam position to acquire both chiral (+) and chiral (–) spectra, while in the APR-EMCD a single detector aperture is sufficient.

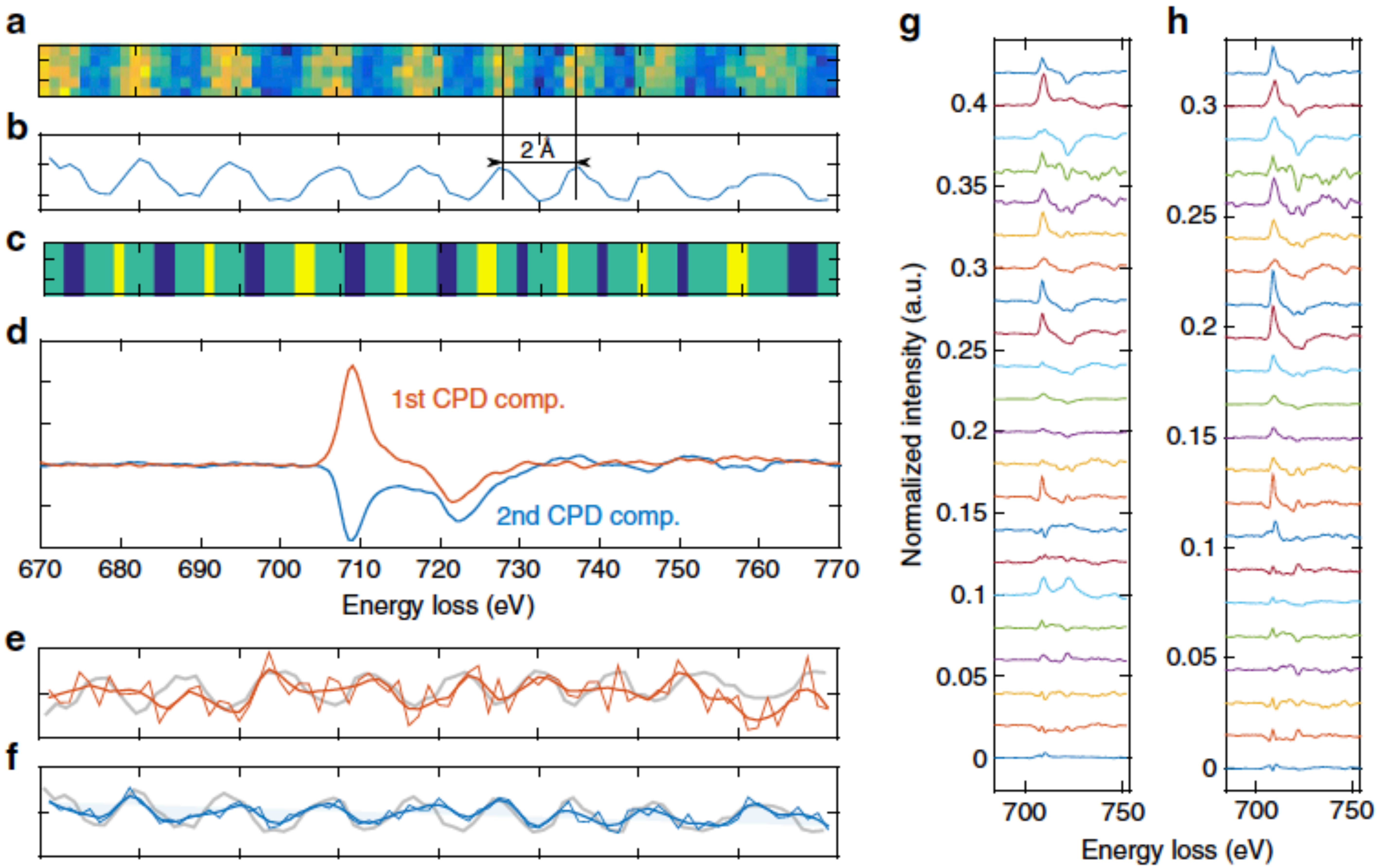

Figure 3 | Experimental detection of APR-EMCD. (**a**) Representative ADF image of the scanned area and (**b**) its line profile. A smoothed profile was used to identify individual minima and maxima, based on which a mask has been defined (**c**) with blue and yellow regions marking summation areas centred at $d/4$ to the right or left of the atomic columns. Their width is determined by local steepness of the ADF line profile. (**d**) Example of the two CPD components with line profiles of their maps. (**e**,**f**) Note the strong correlation between the second CPD component (blue) and the overlayed ADF line profile shown in grey colour. The EMCD-like component also shows such a tendency, but the correlation is weaker. (**g**) Spectral differences obtained before the subtraction of the second CPD component and (**h**) after the subtraction. Note how the subtraction of the second CPD component leads to a higher number of spectra showing clear EMCD signature in (**h**). Spectral differences were calculated from scaled spectra, so that their average peak value at L_3 edge equals to one. In **g** and **h**, the individual spectral differences were vertically offset by 0.02 and 0.015, respectively.

Inelastic scattering - III

Low loss spectroscopy

Cécile Hébert IPHYS-LSME

Layout

- Introduction
- Formalism
- Experiment, plasmon dispersion
- Plural scattering
- beyond linear response
- Surface effects
- Relativistic effects

Layout

- Introduction
- Formalism
- Experiment, plasmon dispersion
- Plural scattering
- beyond linear response
- Surface effects
- Relativistic

Introduction

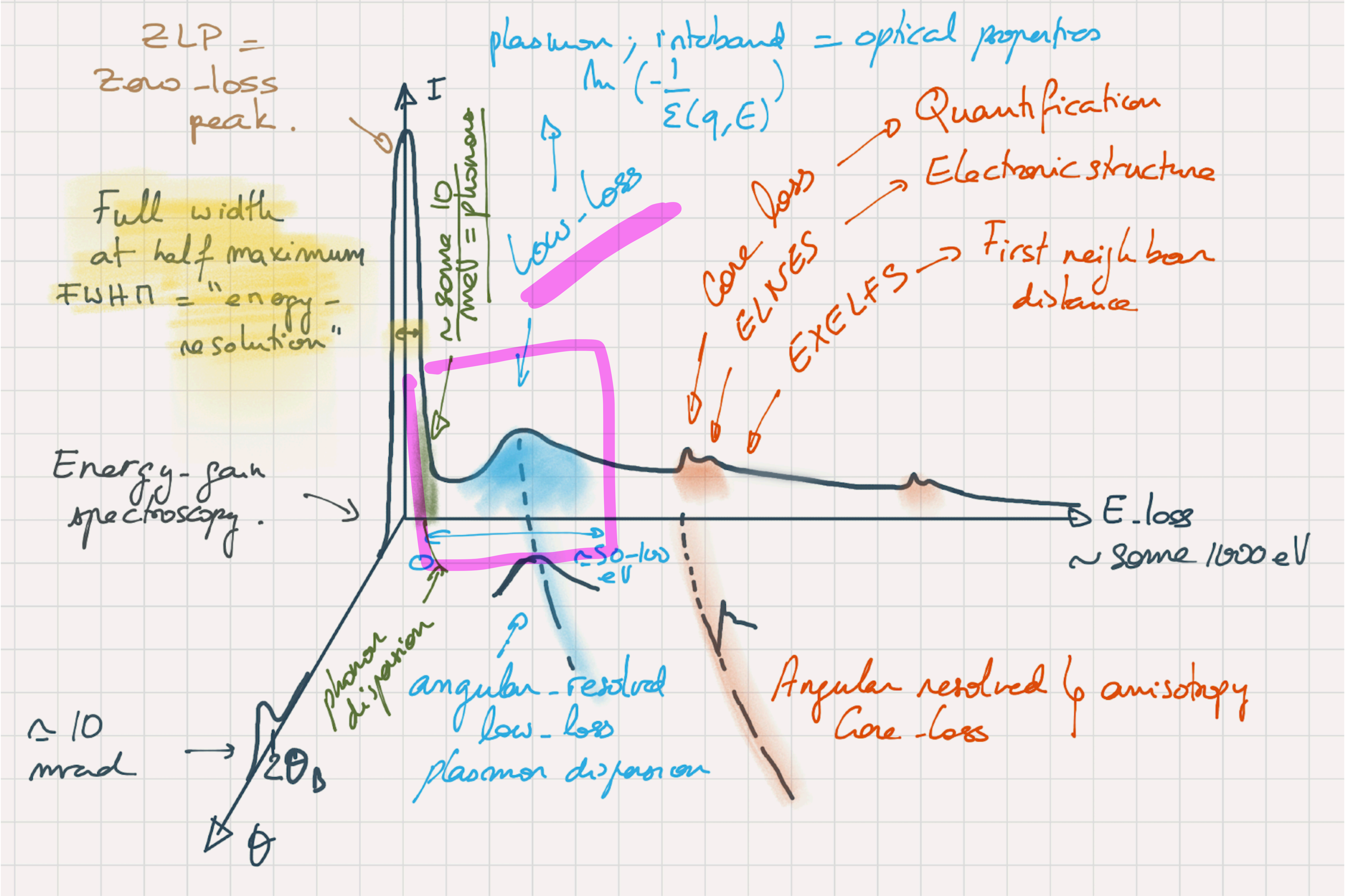

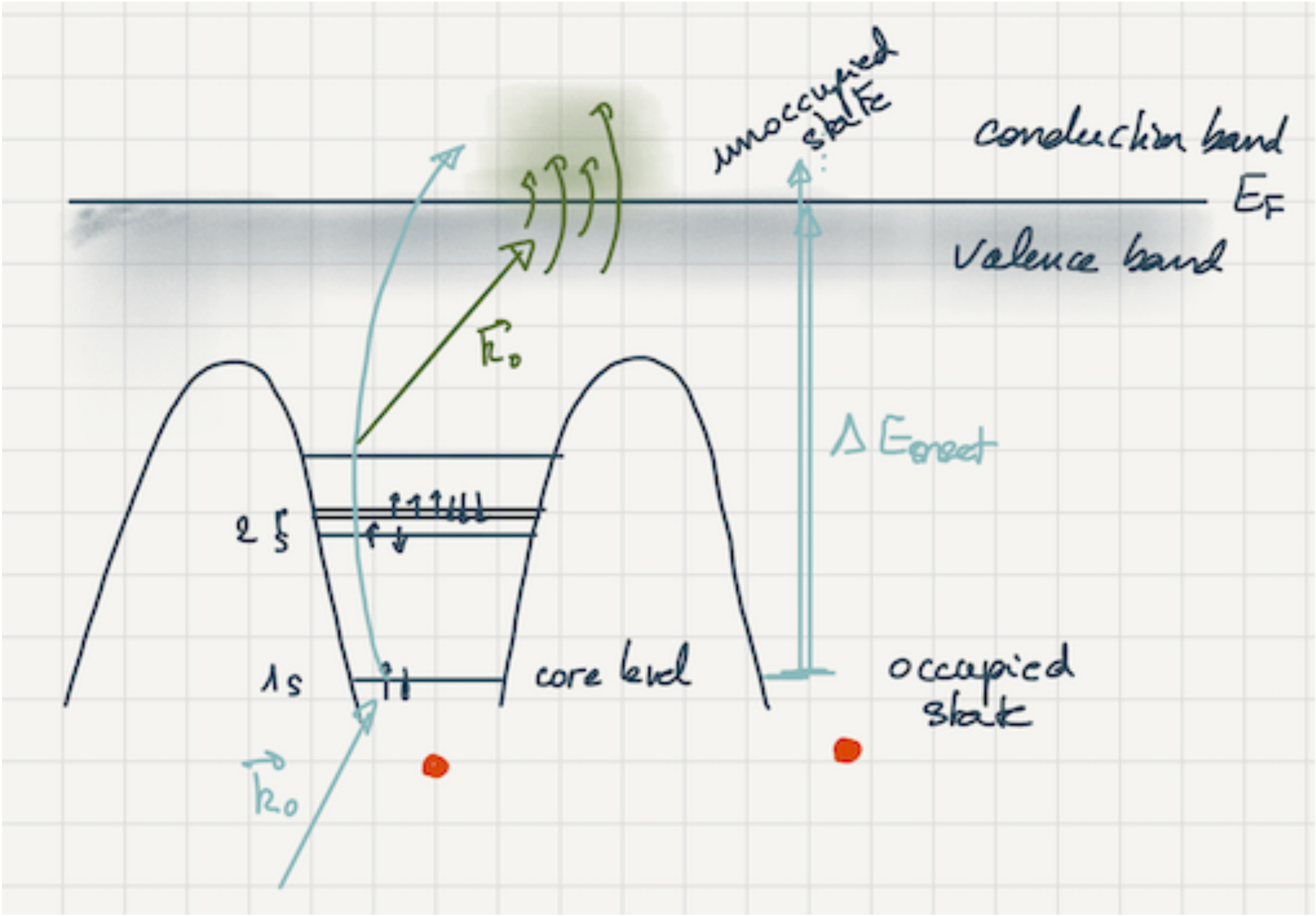

Layout

- Introduction
- Formalism
- Experiment, plasmon dispersion
- Plural scattering
- beyond linear response
- Surface effects
- Relativistic effects

Formalism

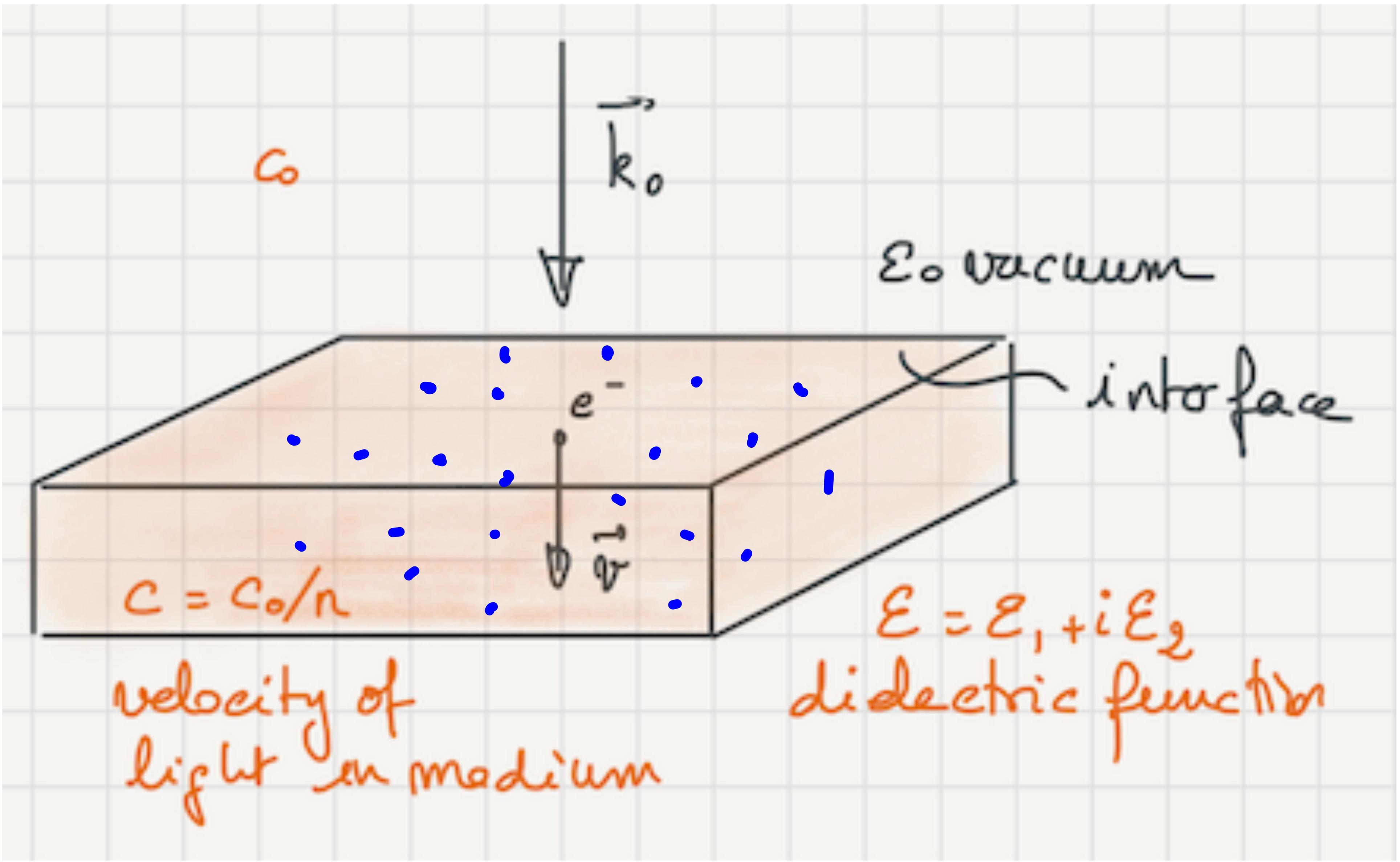

- Single electron description not applicable
- Medium described by the dielectric function
- Linear reaction of medium on the fast travelling charged particle
- ~~Effect of boundaries (surfaces)~~

under the carpet

- ~~Retardation effect (speed of electron versus speed of light)~~

under a 2. carpet

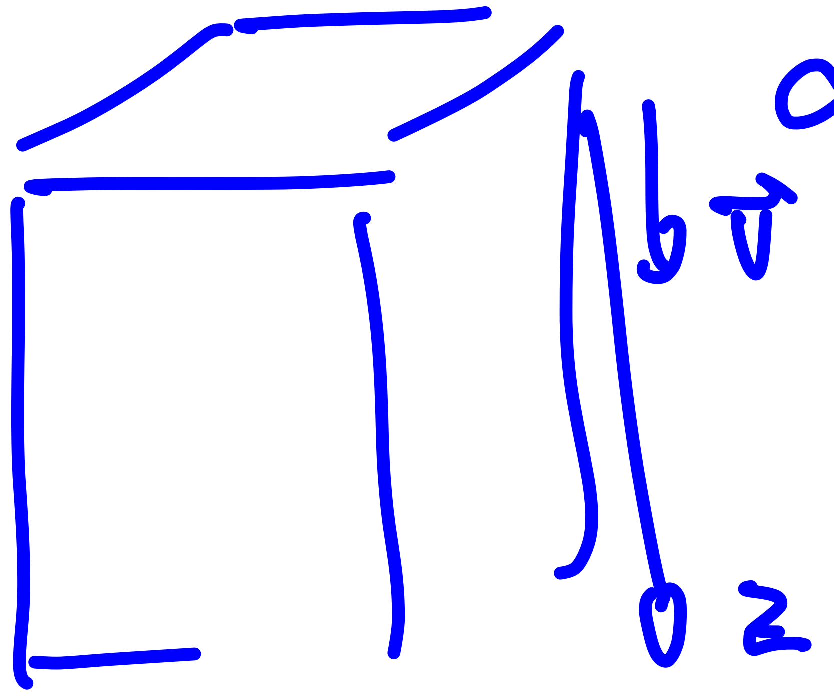

∞ medium

→ energy lost for a distance dz

Formalism

$\vec{v}$ velocity
$\vec{v} // \vec{e}_3$
z

$e^- \rightarrow$ free charge fast e^-
$\leftarrow$ réaction of the medium

Infinite medium; no retardation, linear response

$$\left.\begin{aligned}\overrightarrow{\nabla}\,\overrightarrow{D}(\vec{r},t) &= \rho_f(\vec{r},t) \\ \rho_f(\vec{r},t) &= -e\delta(\vec{r}-\vec{v}t)\end{aligned}\right\}(1+2)$$

divergence of electric displacement linked to density of free charge

Fourier space

$f \rightarrow \tilde{f} = \iint f(\vec{r},t)\, e^{-2\pi i \vec{q}\cdot\vec{r} + i\omega t}$

$\hookrightarrow$ def of $\lambda \Rightarrow k = 1/\lambda$

$$FT[\overrightarrow{\nabla}\,\vec{f}] = 2\pi i\vec{q}\,FT[\vec{f}]$$

FT of (1+2)

$$2\pi i\vec{q}\cdot\overrightarrow{D}(\vec{q},\omega) = \tilde{\rho} = -e\delta(2\pi\vec{q}\cdot\vec{v}-\omega) \quad (3)$$

Maxwell

$$(4)\quad \overrightarrow{D}(\vec{q},\omega) = \underbrace{\epsilon_0\epsilon(\vec{q},\omega)}_{\text{dielectric function of medium}}\overrightarrow{E}(\vec{q},\omega)$$

Response of medium to perturbation

Formalism

Infinite medium; no retardation

$$\overrightarrow{E}(\vec{r},t) = -\overrightarrow{\nabla}\Phi(\vec{r},t)$$ Electric field and potential

FT

(5) $$\overrightarrow{E}(\vec{q},\omega) = -2\pi i\vec{q}\Phi(\vec{q},\omega)$$ fourier space

(3)+(4)+(5)

(6) $$\boxed{\Phi(\vec{q},\omega) = -\frac{e\delta(2\pi\vec{q}\cdot\vec{v}-\omega)}{4\pi^2q^2\epsilon_0\epsilon(\vec{q},\omega)}}$$

Electron travels along z direction, a distance dz=v.dt during dt

experience a force

$\delta W = \vec{F}_{orce} \cdot d\vec{r}$

$= \vec{F}_{orce} \cdot dz\,\vec{e}_z$

Stopping power $SP = \frac{-\cancel{d}\,\delta W}{dz}$ with ~~d~~ δW work of electric force over distance dz

Force $= -\vec{\nabla}\phi$ $\quad \frac{\partial \phi}{\partial z}$ (only over z direction)

Formalism

Infinite medium; no retardation

$$SP = -e\frac{\partial \Phi}{\partial z}\bigg|_{x=y=0,z=vt}$$

Back to real space…

$\vec{r} = z\vec{e_z}$

$\vec{q}\cdot\vec{v}$ $\quad \vec{v} = v\vec{e_z}$

FT of (G)

$$\Phi(\vec{r},t) = \underbrace{\int}_{\text{space}}\underbrace{\int}_{\text{time}} -\frac{e\delta(2\pi\vec{q}\cdot\vec{v}-\omega)}{4\pi^2 q^2\epsilon_0\epsilon(\vec{q},\omega)}e^{2\pi i\vec{q}\vec{r}-i\omega t}d^3q d\omega$$

$$\vec{q}\cdot\vec{v} = vq_z$$

$$SP = \frac{e^2}{4\pi^2\epsilon_0}\int\int 2\pi i q_z\frac{\delta(2\pi v q_z-\omega)}{(q_\perp^2+q_z^2)\epsilon(\vec{q},\omega)}e^{2\pi i\vec{q}\vec{r}-i\omega t}d^3q d\omega\bigg|_{x=y=0,z=vt}$$

$$\int_{q_z}\int_{q_\perp}\int_{\text{time}\ \omega=-\infty}^{+\inf}$$

integration over qz with delta function picks value of integrand (normalize by $2\pi v$)

Formalism

Infinite medium; no retardation

$$SP = \frac{e^2 i}{8\pi^3 \epsilon_0 v^2} \int_{q_\perp} \int_{\omega=-\infty}^{+\infty} \frac{\omega}{(q_\perp^2 + (\frac{\omega}{2\pi v})^2)\epsilon(\vec{q}_\perp, \omega)} d^2 q_\perp d\omega$$

$$\int_{\omega=-\infty}^{+\infty} = \int_{\omega=-\infty}^{0} + \int_{\omega=0}^{+\infty}$$

$\epsilon(\vec{r}, t)$ real therefore $\epsilon(-\omega) = \epsilon^*(\omega)$

$$SP = \frac{e^2}{4\pi^3 \epsilon_0 v^2} \int_{q_\perp} \int_{\omega=0}^{+\infty} \frac{\omega}{(q_\perp^2 + (\frac{\omega}{2\pi v})^2)} \Im \frac{-1}{\epsilon(\vec{q}, \omega)} d^2 q_\perp d\omega$$

$$\Delta E = \hbar\omega$$

Formalism

Infinite medium; no retardation

$$SP = \frac{e^2}{4\pi^3\epsilon_0 v^2}\int_{q_\perp}\int_{\omega=0}^{+\infty}\frac{\omega}{(q_\perp^2 + (\frac{\omega}{2\pi v})^2)}\Im\frac{-1}{\epsilon(\vec{q},\omega)}d^2q_\perp d\omega$$

$$SP = \int\int \Delta E \frac{\partial P}{\partial q_\perp \partial\omega} d^2 q_\perp d\omega$$

P: E-loss probability per unit path length

$$SP = \int\int \underbrace{n_v}_{\text{number of atoms per unit volume}} \Delta E \frac{\partial\sigma}{\partial\Omega\partial\Delta E} d\Omega d\Delta E$$

$$\boxed{\frac{\partial^2\sigma}{\partial\Omega\partial\Delta E} = \frac{e^2}{n_v\pi h^2\epsilon_0 v^2}\frac{1}{\theta^2+\theta_E^2}\Im\left(\frac{-1}{\epsilon(\vec{q},\Delta E)}\right)}$$

Formalism

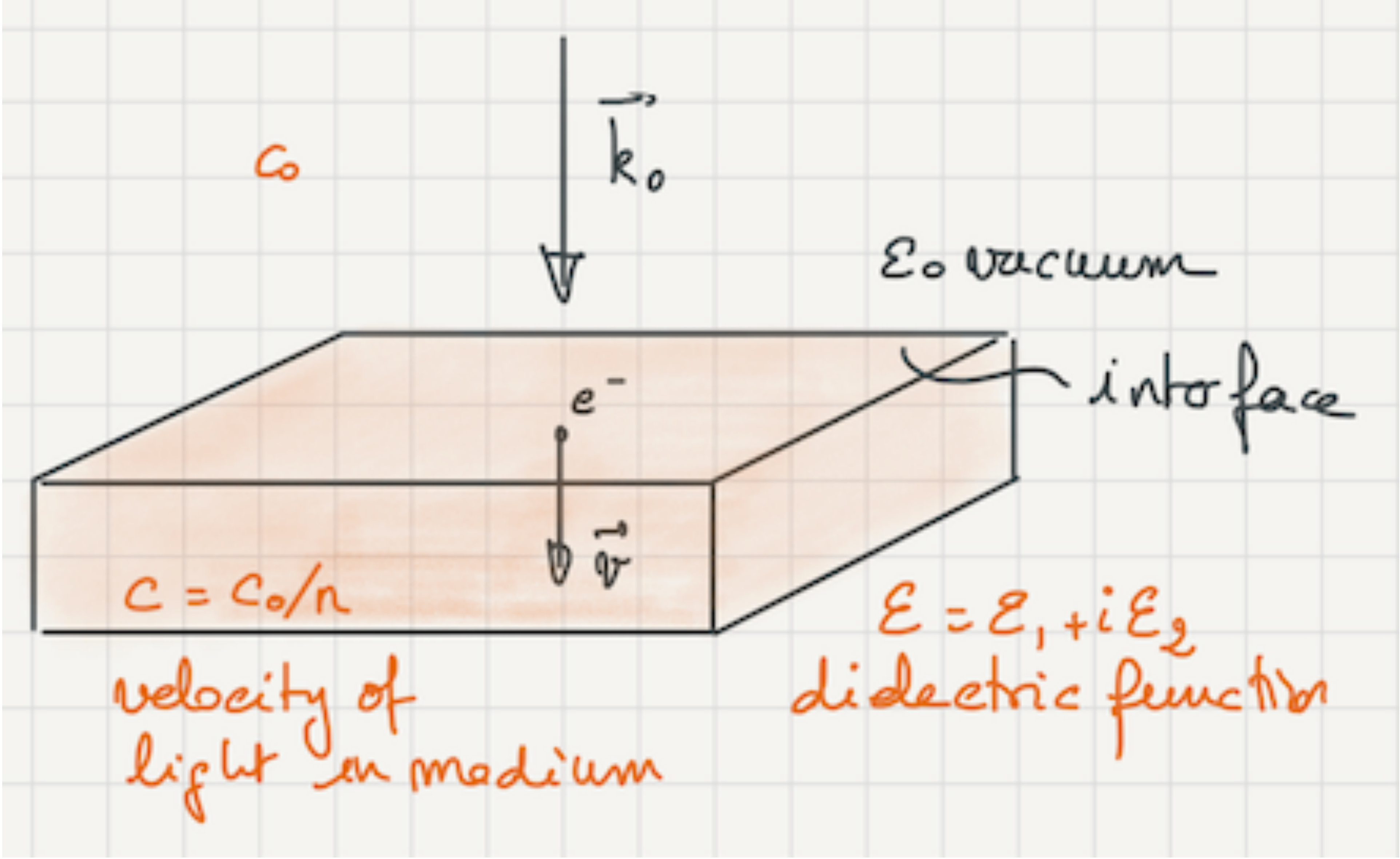

- Single electron description not applicable
- Medium described by the dielectric function
- Linear reaction of medium on the fast travelling charged particle
- Effect of boundaries (surfaces)
- Retardation effect (speed of electron versus speed of light)

$$\frac{\partial^2\sigma}{\partial\Omega\partial\Delta E} = \frac{e^2}{n_v \pi h^2 \epsilon_0 v^2}\frac{1}{\theta^2+\theta_E^2}\Im\left(\frac{-1}{\epsilon(\vec{q},\Delta E)}\right)$$

$\varepsilon_1 + i\,\varepsilon_2$

Formalism

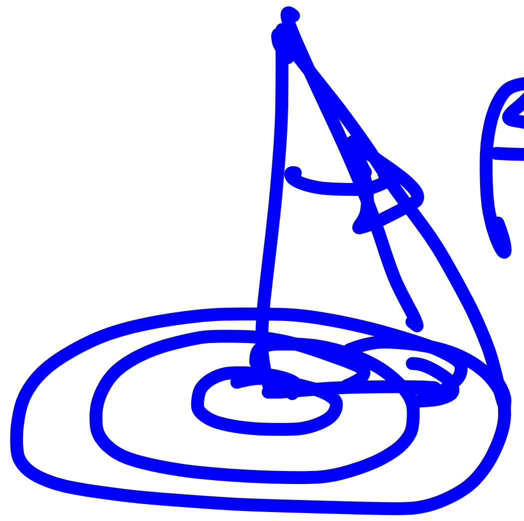

+ assumption $\ln\left(\frac{-1}{\varepsilon}\right)$ does not change too much with $\vec{q}$

$$\frac{\partial^2\sigma}{\partial\Omega\partial\Delta E} = \frac{e^2}{n_v \pi h^2 \epsilon_0 v^2}\frac{1}{\theta^2 + \theta_E^2}\Im\left(\frac{-1}{\epsilon(\vec{q}, \Delta E)}\right)$$

$$\frac{\partial\sigma}{\partial\Delta E} = \frac{e^2}{n_v h^2 \epsilon_0 v^2}\ln(1 + \beta^2/\theta_E^2)\Im\left(\frac{-1}{\epsilon(\vec{q}, \Delta E)}\right)$$

single scattering distribution.

$$SSD = \left(\frac{e^2}{\pi h^2 \epsilon_0 v^2}\right)D\frac{1}{\theta^2 + \theta_E^2}\Im\left(\frac{-1}{\epsilon(\vec{q}, \Delta E)}\right)$$

→ Kramers Kronig analysis

→ $\mathrm{Re}\left(-\frac{1}{\varepsilon}\right)$

→ ε_1 & ε_2

↳ n r ....

all optical properties!

= D thickness of sp.

Layout

- Introduction
- Formalism
- Experiment, plasmon dispersion
- Plural scattering
- beyond linear response
- Surface effects
- Relativistic effects

Experiment

PHYSICAL REVIEW B VOLUME 27, NUMBER 9 1 MAY 1983

Experimental energy-loss function, $\mathrm{Im}[-1/\epsilon(q,\omega)]$, for aluminum

P. E. Batson* and J. Silcox

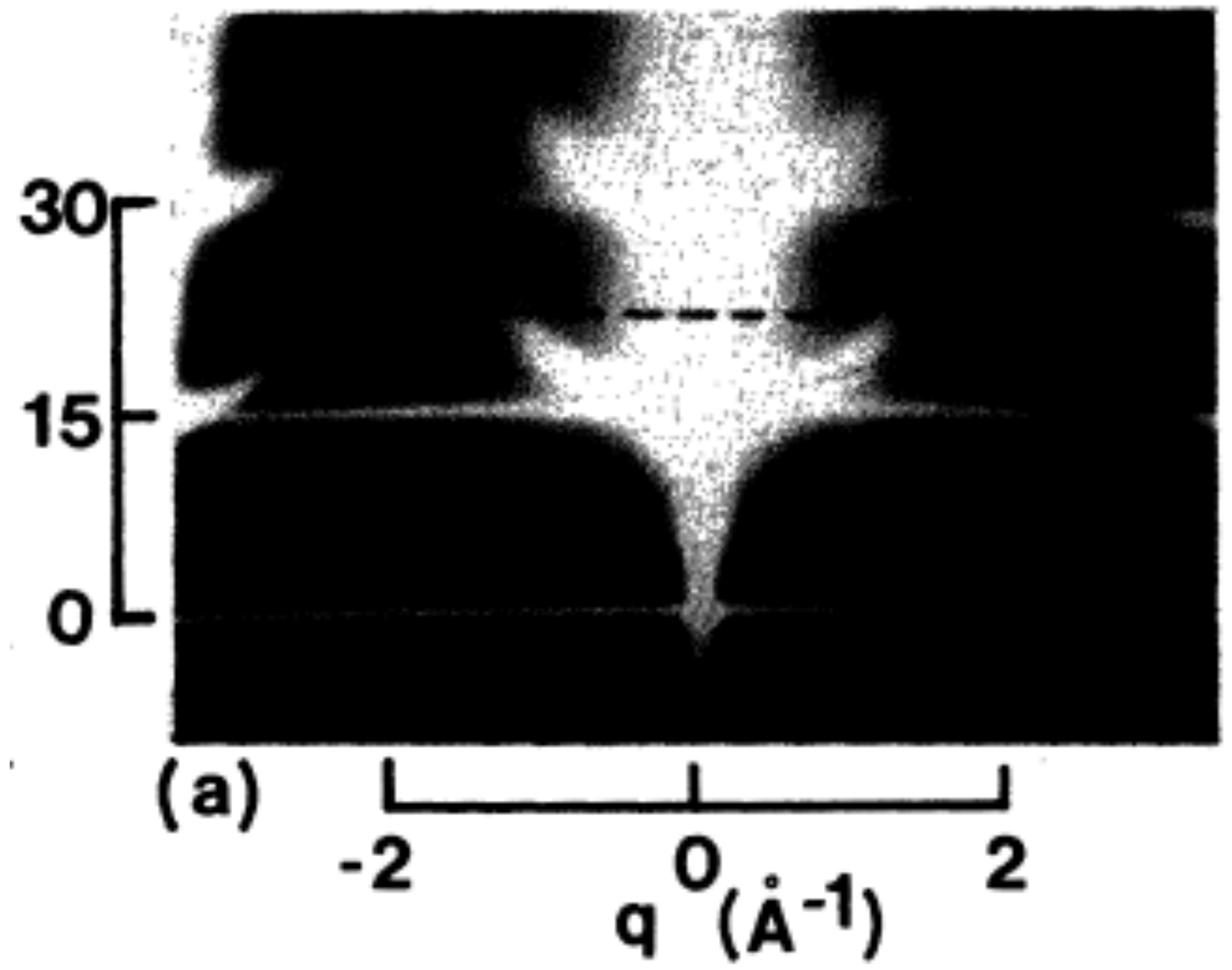

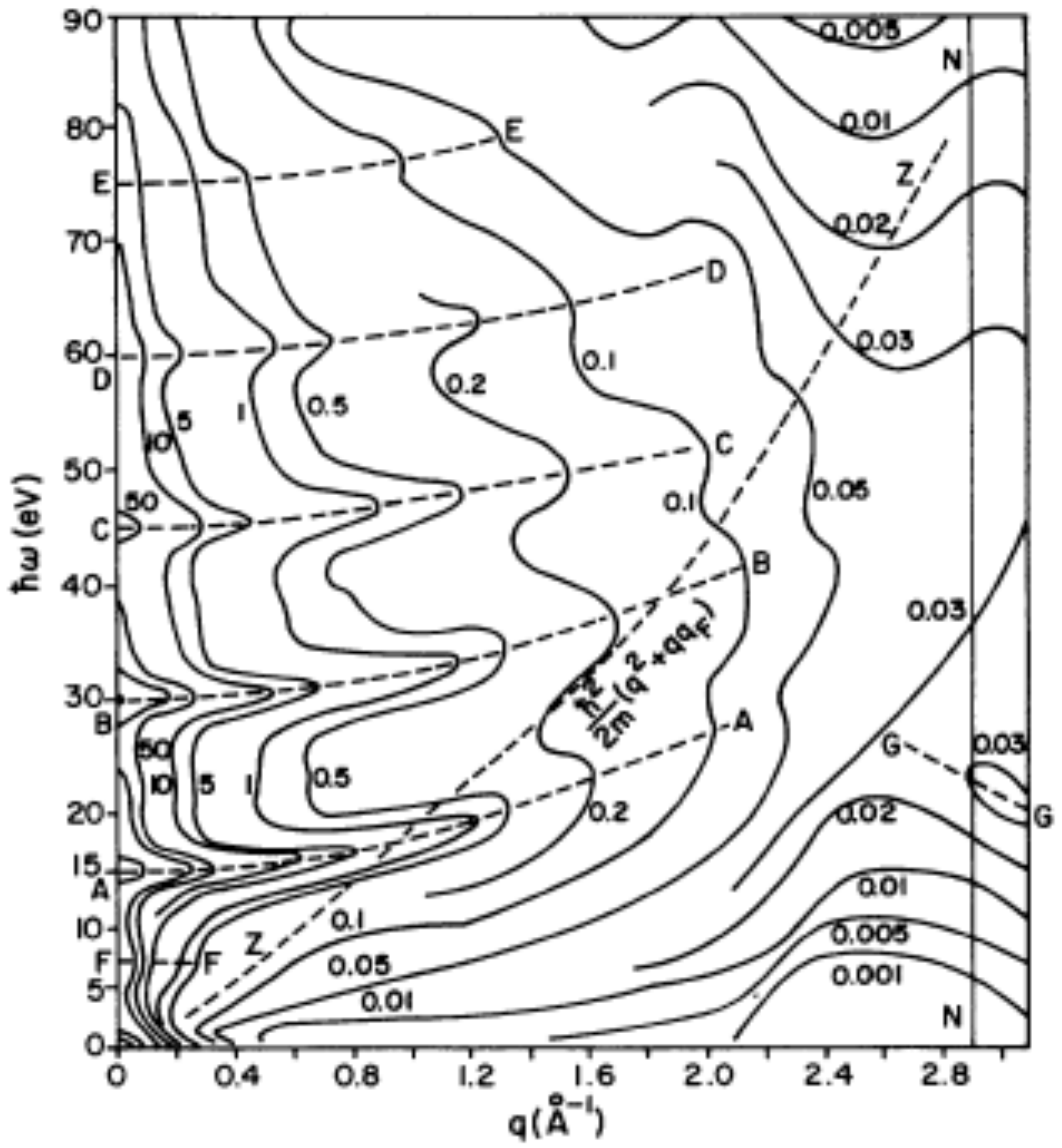

FIG. 11. Intensity contour map after application of the image subtraction. Note the enhancement of the Bragg plus plasmon scattering (GG).

Free electron gaz: Jellium model

damped oscillator.

Plasmon parabolic dispersion

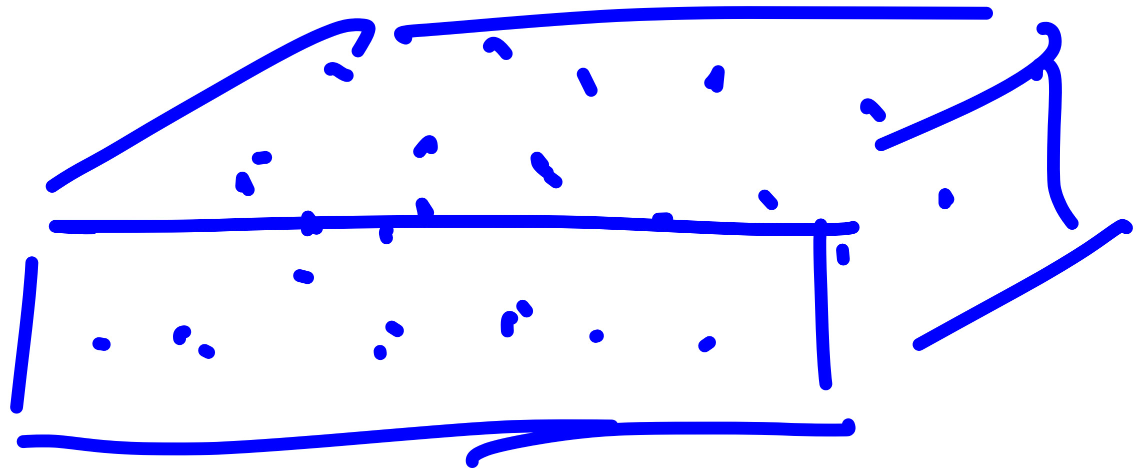

Experiment interpretation

Jellium model: FEG modelled as a damped oscillator, with Γ damping constant.

natural frequency of damped oscillator can be calculated $\omega_p = \sqrt{ne^2/(\epsilon_0 m)}$

sharp resonance: peak at ω_p. Broad resonance, peak appears at lower energy

resonance for zero-crossing of ϵ_1 and small ϵ_2

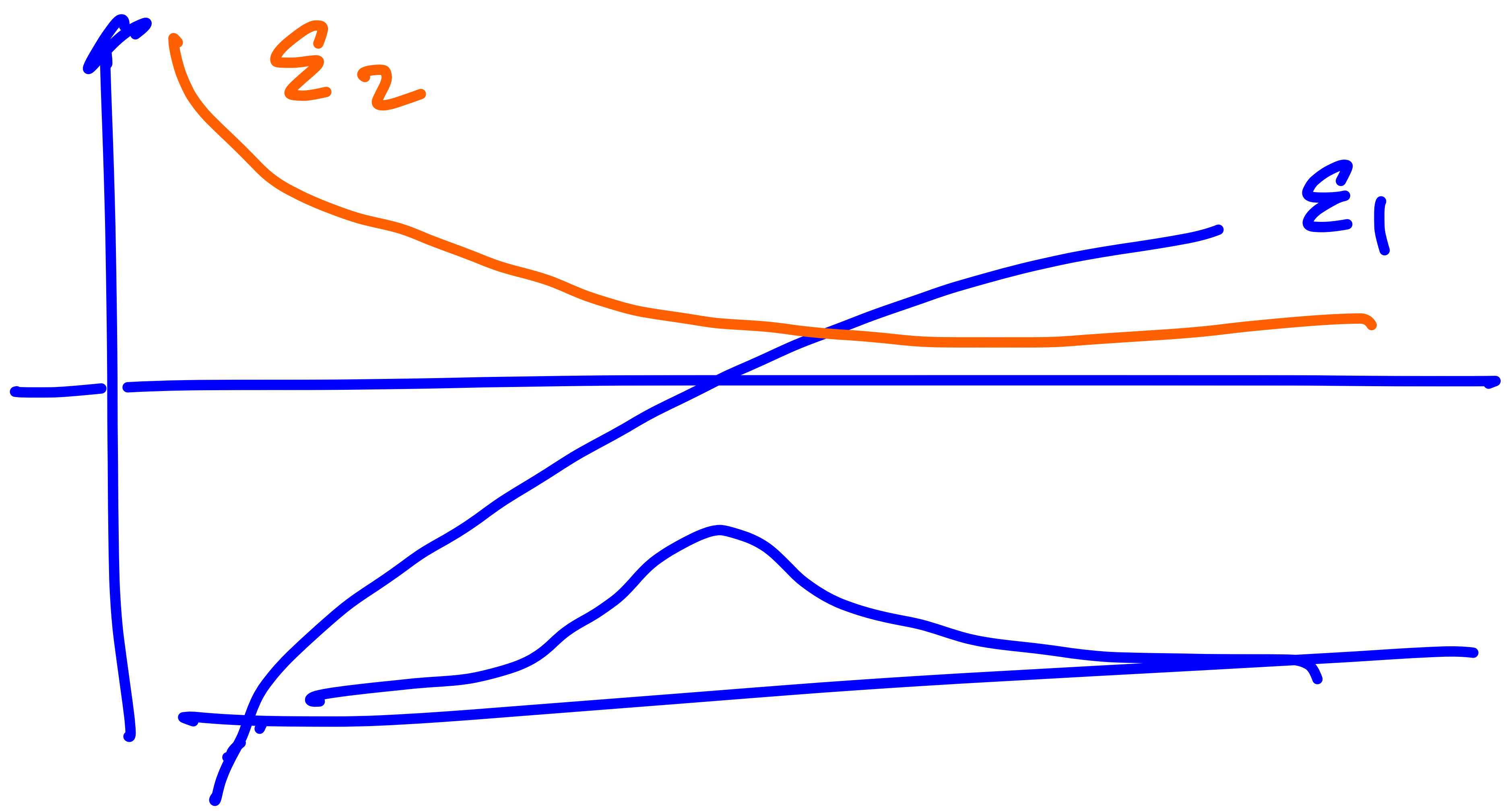

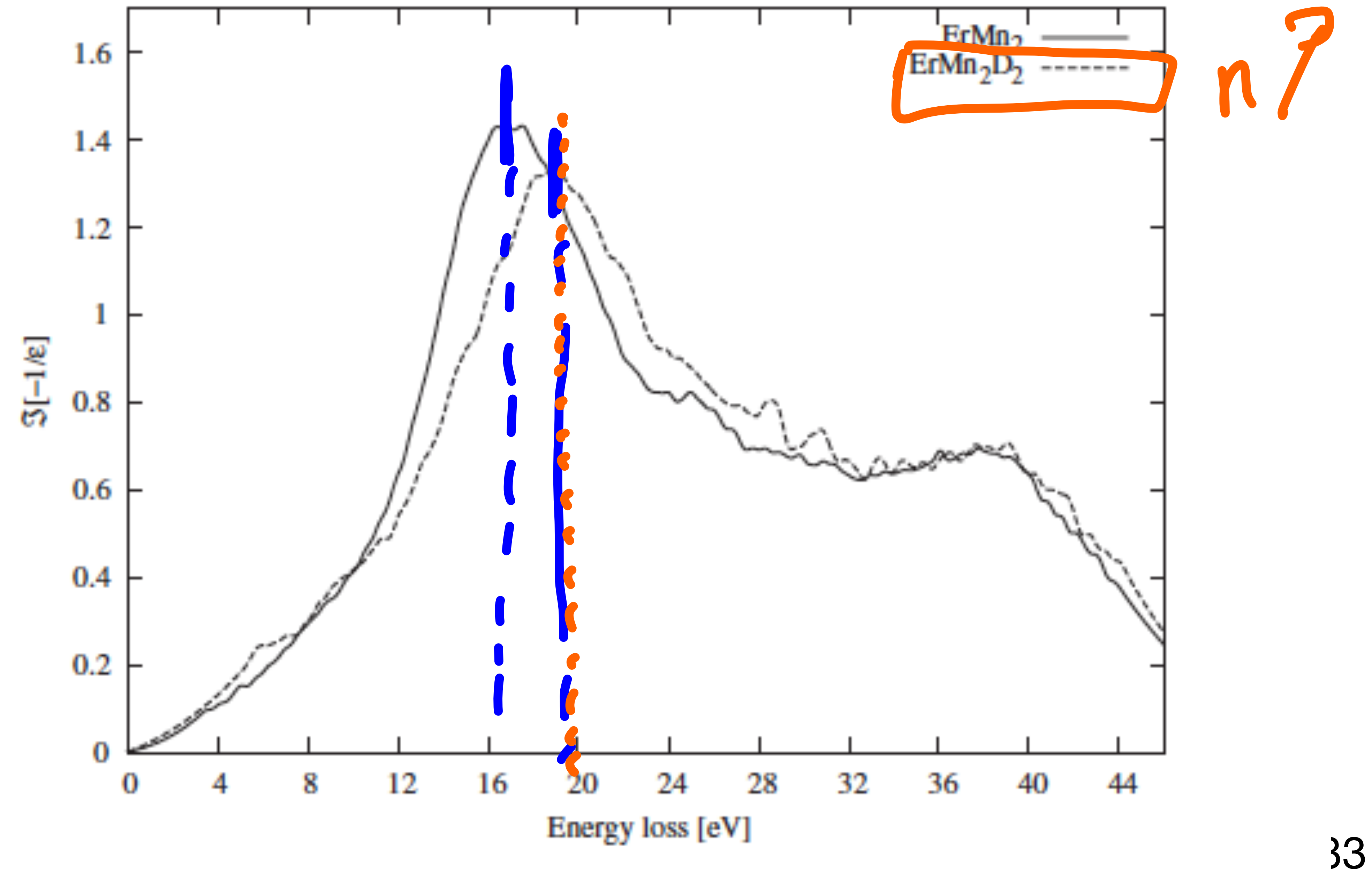

Experiment

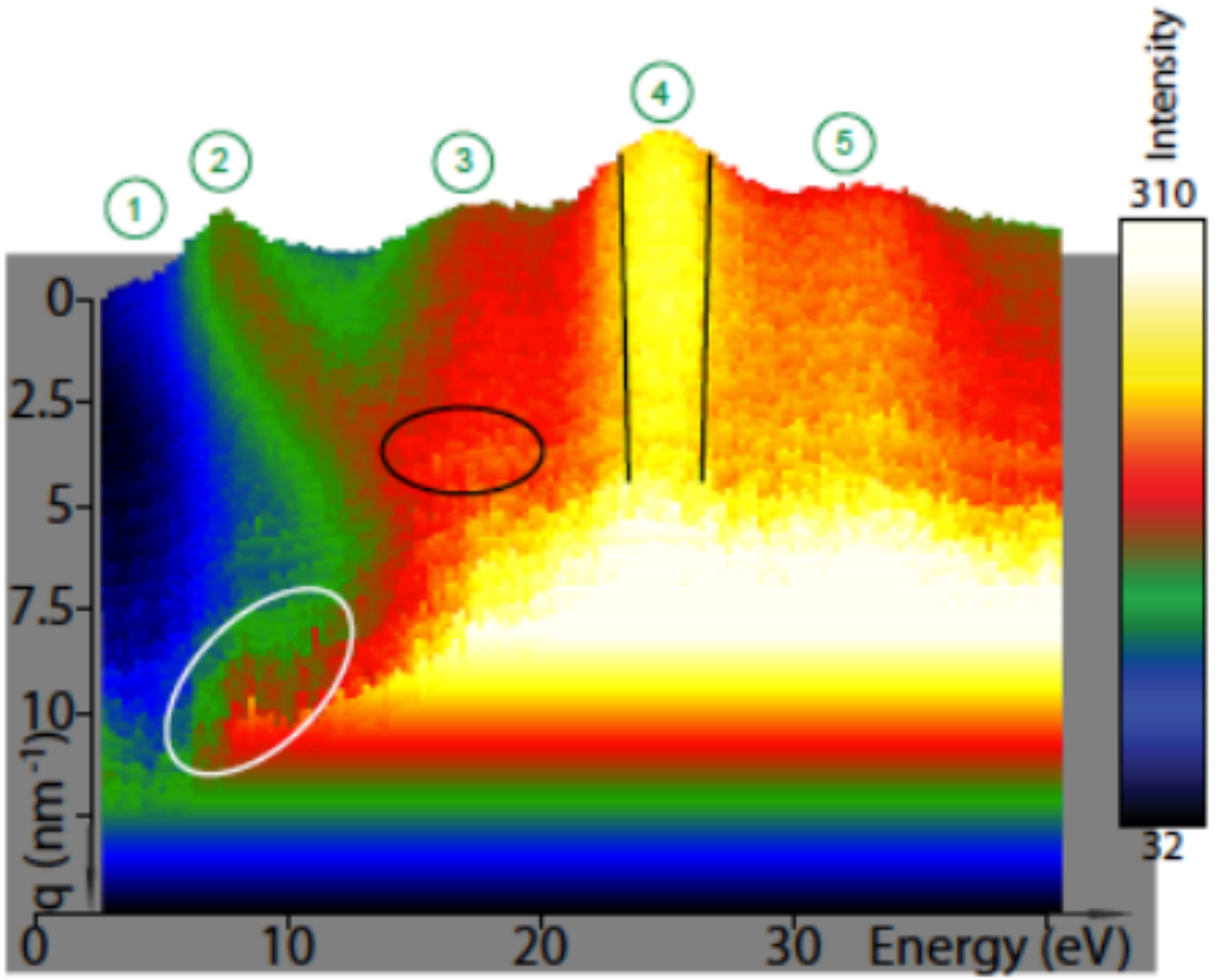

Experiment in Ag

structure 2 shows a nice dispersion

other structures have a different behaviour

Simulation: TDDFT